Composites Science and Technology 150 (2017) 141–166

Contents lists available at ScienceDirect

Composites Science and Technology

journal homepage: http://www.elsevier.com/locate/compscitech

Learning from nacre: Constructing polymer nanocomposites

Chuanjin Huang, Qunfeng Cheng*

Key Laboratory of Bio-Inspired Smart Interfacial Science and Technology of Ministry of Education, School of Chemistry, Beijing Advanced Innovation Center for Biomedical Engineering, Beihang University, Beijing 100191, China

ARTICLE INFO

Article history:
Received 23 April 2017
Received in revised form
16 July 2017
Accepted 24 July 2017
Available online 26 July 2017

Keywords:
Polymer nanocomposites
Layered structures
Mechanical properties
Interface
Synergism

ABSTRACT

Due to the small size and special physical properties of nanometer materials, polymer nanocomposites, combined nanoscale reinforcements with polymer matrix, possess outstanding mechanical properties and functional performances, which play a key role in many fields, especially for application in fields of industry and aerospace. However, poor dispersion and weak interfacial interactions are the critical factors that restrict the great improvement in performance of polymer nanocomposites. Although these issues have been solved in some extent *via* various methods, such as surfactant adsorption, polymer wrapping, surface modification, it still remains a great challenge for achieving high performance polymer nanocomposites as theoretically expected. Nacre, with 95% (volume fraction) inorganic calcium carbonate and 5% (volume fraction) biopolymers, is a typical binary cooperative complementary material system with hard inorganic component and soft organic matrix. Its typical "brick-and-mortar" hierarchical micro/nano-scale structure provides an excellent guideline for constructing polymer nanocomposites. It skillfully overcomes the bottleneck of traditional approaches for fabricating polymer nanocomposites, such as poor dispersion, low loading, and weak interfacial interactions. Recently, we have successfully demonstrated the bioinspired concept is a successful approach for constructing high performance polymer nanocomposites based on different reinforcement fillers, such as nanoclay, carbon nanotubes, and graphene. The resultant bioinspired polymer nanocomposites (BPNs) show layered hierarchical micro/nano-scale structure and outstanding mechanical properties. This feature article reviews our group's work and other groups' research results on BPNs in recent years, and discuss the advantages of BPNs through comparing with traditional methods, as shown in Fig. 1, including: i) Bioinspired assembly approaches for achieving the homogeneous dispersion and layered structure of reinforcement fillers in polymer matrix, such as layer-by-layer, infiltration, evaporation, freeze casting.; ii) various approaches for designing interfacial interactions; iii) the effect of synergy on the performance of BPNs; iv) representative applications of BPNs, such as energy storage devices, filter, sensors. Finally, this feature article also focuses on a perspective of BPNs, commenting on whether the bioinspired concept is viable and practical for polymer nanocomposites, and on what has been achieved to date. Most importantly, a roadmap of BPNs for near future will be depicted, including integrated mechanical properties and functions, intelligent properties, etc.

1. Introduction

Nanocomposites, coined by Roy, Komarneni and colleagues [1], are novel materials where at least one of the components ranges from 1 to less than 100 nm [2,3]. They are widely spread over the biological systems, like plants, bone and nacre [2]. Due to the surface effect, small size effect, the tunnel effect of macroscopic quantum and the effect of quantum size of nanoscale as nanofillers, the physical, chemical properties of nanocomposites are superior to traditional composites [4]. With the development of nanoscience and nanotechnology, tremendous nanocomposites have been made in the past decades, for example, polymer nanocomposites are rapidly developed as one of the most promising materials in the 21st century.

1.1. Polymer nanocomposites

Because of unique attributes of polymer such as easy production

* Corresponding author.
E-mail address: cheng@buaa.edu.cn (Q. Cheng).

http://dx.doi.org/10.1016/j.compscitech.2017.07.021
0266-3538/

and processing, lightweight, it is widely used in many fields. However, compared with metals, polymer shows low strength and toughness [5]. In order to improve the mechanical properties and other performances of polymer, nanofillers such as montmorillonite (MMT) [6], carbon nanotubes (CNTs) [7,8], graphene [9], are blended into the polymer matrix to fabricate polymer nanocomposites. Therefore, the polymer nanocomposites exhibit excellent physical properties such as mechanical [10,11], flame-retardant [6,12], barrier [13] and electrical properties [8,14]. MMT as widely used nanofiller can remarkably increase mechanical properties of polymer nanocomposites when blended into polymer [15]. For example, Chen et al. [16] demonstrated that 8 wt% addition of MMT to poly (ϵ-caprolactone) (PCL) resulted in 50% improvement in the tensile modulus of resultant nanocomposites. However, MMT-based polymer nanocomposites can be compromised in flexibility due to the stiff nature and poor dispersion of MMT [6]. Carbon nanomaterials such as CNTs and graphene with high mechanical and electrical properties [8] have been paid more attention to prepare integrated multifunctional polymer nanocomposites.

Since CNTs were discovered by Iijima in 1991 [17], they show promising performance, including outstanding mechanical and electrical properties, which have been attempted to prepare polymer nanocomposites by Ajayan in 1994 [14]. CNTs-based polymer nanocomposites are rapidly developed in recent decades. Liu et al. [18] prepared functionalized CNTs-poly vinyl alcohol (PVA) nanocomposites and achieved a 78% improvement of the tensile modulus *via* addition of 0.8 wt% of functionalized CNTs. Although CNTs array based polymer nanocomposites have shown much higher mechanical properties [19–22], it remains great challenges to achieve high performance CNTs-based polymer nanocomposites.

Graphene, the strongest material ever measured and best electrical property, is ideal nanofiller to fabricate polymer nanocomposites [23]. Since it was first reported in 2006 by Stankovich [24], the studies on graphene-based nanocomposites are rapidly grown in recent years [9]. Liang et al. [25] fabricated graphene oxide (GO)-PVA nanocomposites *via* a simple water solution processing method, achieving 76% and 62% improvement in tensile strength and Young's modulus, respectively, with only addition of 0.7 wt% of GO nanosheets. The mechanical properties of polymer nanocomposites were theoretically predicted to be further improved with increasing the content of nanofillers [26]. However, the issues are arising with adding much more nanofillers, such as poor dispersion, low loading and weak interfacial interactions [27], restricting the great improvement in performances of traditional polymer nanocomposites (TPNs). Until now, it remains a great challenge to solve these issues and reach high performance polymer nanocomposites. While, natural materials, such as bone, bamboo and nacre [28], assembled by two or more components, are also typical nanocomposites and show unique mechanical properties, providing novel inspiration for constructing high performance polymer nanocomposites. Compared with TPNs, the natural nanocomposites contain much higher loading of nanofillers, which is a roadblock for TPNs.

1.2. Bioinspired strategy for polymer nanocomposites

Numerous investigations have revealed that the unique mechanical properties of natural materials are attributed to two factors: one is fine architecture and the other one is abundant interfacial interactions [28]. For example, nacre, composed of 95 vol % aragonite platelets and 5 vol % biopolymers, is a typical binary cooperative complementary material system, and shows a “brick-and-mortar” hierarchical micro/nano-scale structure [29], providing an excellent guideline for constructing polymer nanocomposites. It skillfully overcomes the bottleneck of traditional approaches for fabricating polymer nanocomposites, such as poor dispersion, low loading, and weak interfacial interactions.

The purpose of investigating the structure and properties of nacre is to construct novel high performance bioinspired polymer nanocomposites (BPNs). Building blocks as main components are very essential for the mechanical properties of BPNs [30,31]. The typical two-dimensional (2D) nanosheets, such as flattened double-walled carbon nanotubes (FDWCNTs) [32], MMT [33,34], graphene oxide (GO) [23], layered double hydroxides (LDHs) [35], alumina flakes [36], and $CaCO_3$ [37], have been utilized as building blocks to prepare high performance BPNs. In the following section, we mainly describe CNTs, MMT and GO, as shown in Fig. 2.

CNTs show extremely high tensile strength (~100 GPa) and Young's modulus (~1000 GPa) [14], which are suitable for constructing polymer nanocomposite [38]. Recently, Cheng et al. [32] synthesized FDWCNTs, and assembled FDWCNTs into layered nanocomposite with epoxy matrix, as shown in Fig. 2A. This bioinspired strategy can reach high CNTs loading in the nanocomposites, for example, the FDWCNTs content is 70 wt%, higher than other CNTs-based nanocomposites. Meanwhile, the layered structure is also easily achieved. However, the interface interaction between CNTs and polymer matrix is limited to be designed due to inertness of the CNTs.

MMT with abundant interfacial functional groups can form strong interfacial interactions with polymer [6]. The tensile strength and Young's modulus of MMT are 500–700 MPa and 400 GPa, respectively, which are higher than $CaCO_3$ platelets [30]. For example, the Podsiadlo et al. [39] demonstrated ultrastrong and stiff layered MMT reinforced PVA nanocomposites with tensile strength of 400 MPa, and Young's modulus of 107 GPa. These extraordinary mechanical properties are attributed to finely layered architecture and covalent and hydrogen bonding between MMT and PVA. Recently, Wang et al. [33] demonstrated nacre-inspired ternary layered structure of MMT-NFC-PVA nanocomposites, which possess integration of high strength, toughness, and fatigue resistant properties together, as shown in Fig. 2B. Unfortunately, when MMT content of polymer nanocomposites exceeds 70 wt% [26], the MMT nanosheets are easily to be tactoid, leading to the poor dispersion and random structure of the resultant nanocomposites.

GO nanosheets with the tensile strength of 63 GPa and Young's modulus of 500 GPa, prepared by modified Hummers' method, contain abundant functional groups on the surface [9,30], which are one of the best candidates for constructing BPNs different interfacial interactions such as hydrogen bonding [40], ionic bonding [41], π-π interaction [42] and covalent bonding [23]. Compared to CNTs and MMT, the content of GO in the BPNs can be achieved as high as 95 wt%. Furthermore, the graphene-based BPNs can be designed *via* synergistic effects from interfacial interactions and building blocks, as shown in Fig. 2C.

2. Preparation of polymer nanocomposites

The methods of fabricating polymer nanocomposites directly affect the properties of nanocomposites [27]. Herein, several traditional methods for preparing TPNs and bioinspired assembly approaches for fabricating BPNs are discussed. As shown in Fig. 1, the bioinspired approaches demonstrated several advantages compared with traditional methods, such as well dispersion, alignment structure, high content and designable interfacial interactions. In the following sections, the details about the

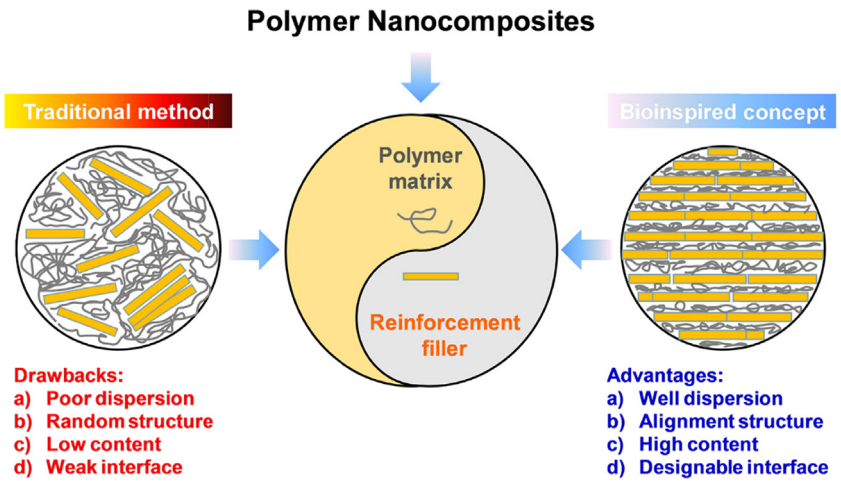

Fig. 1. Comparison of fabrication approaches for polymer nanocomposites. Bioinspired concept shows several advantages, such as well dispersion, alignment, high content of reinforcement fillers, and designable interface with polymer matrix.

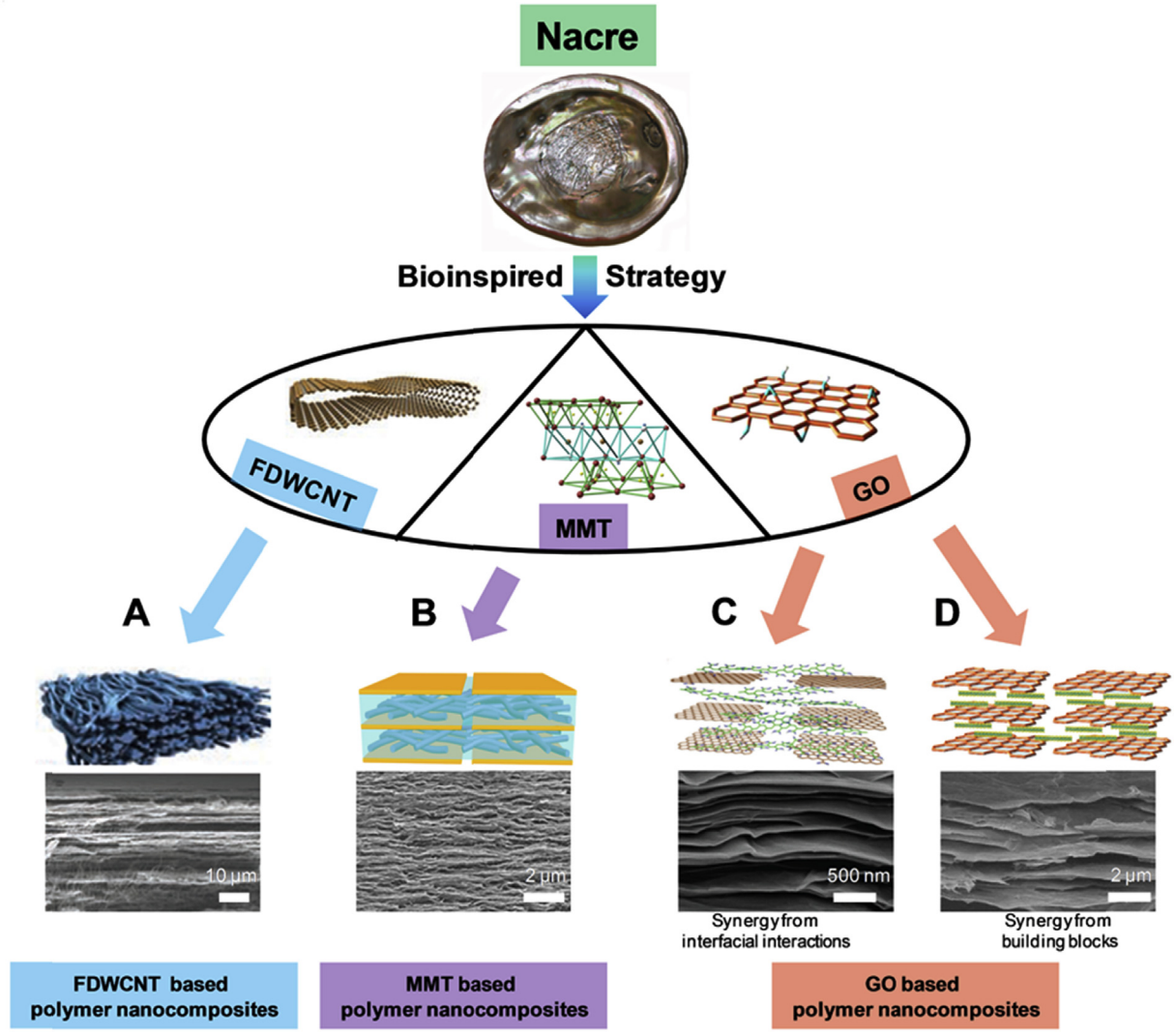

Fig. 2. Bioinspired strategy is used for preparing BPNs with different building blocks as follows: (A) Flattened double-walled carbon nanotubes (FDWCNT) based polymer nanocomposites. FDWCNT could realize layered ordered structure with high content (~70 wt %) in BPNs. Reproduced with permission [32] (B) Montmorillonite (MMT) based polymer nanocomposites. MMT is commonly used to prepare BPNs with high content of building blocks. Reproduced with permission [33]. (C) and (D) Graphene oxide (GO) based polymer nanocomposites. Synergy from interfacial interactions and building blocks is utilized for constructing high performance GO-based BPNs. Reproduced with permission [93,94].

traditional methods and bioinspired approaches are discussed.

2.1. Traditional methods

In past two decades, many preparation methods are developed for constructing polymer nanocomposites, which are mainly categorized into following as: (i) solution mixing [43], melt mixing [44], in-situ polymerization [45,46] and other methods [46]. The process of these approaches is illustrated by the cartoon in Fig. 3. In the following section, these approaches are discussed in detail.

2.1.1. Solution mixing

Solution mixing is a facile and effective method for fabricating polymer nanocomposites [24,27], which has been utilized for different nanofillers. The whole process could be illustrated into three steps, as shown in Fig. 3A. First, the nanofillers are well dispersed in some solution, and the polymer also needs to be dispersed into solution. Then both nanofillers and polymer solution are mixed together through sonication or other mechanical stirring approaches. Finally, the well dispersed mixing solution is evaporated to remove the solvent, and the TPNs are obtained [27]. For example, Geng et al. [43] fabricated nanocomposites of fluorinated single-walled carbon nanotubes (F-SWNTs) dissolved in 2-propanol and poly (ethylene oxide) (PEO), a semi-crystalline thermoplastic polymer. The resultant nanocomposites showed great improvement in tensile strength compared to the pure PEO after

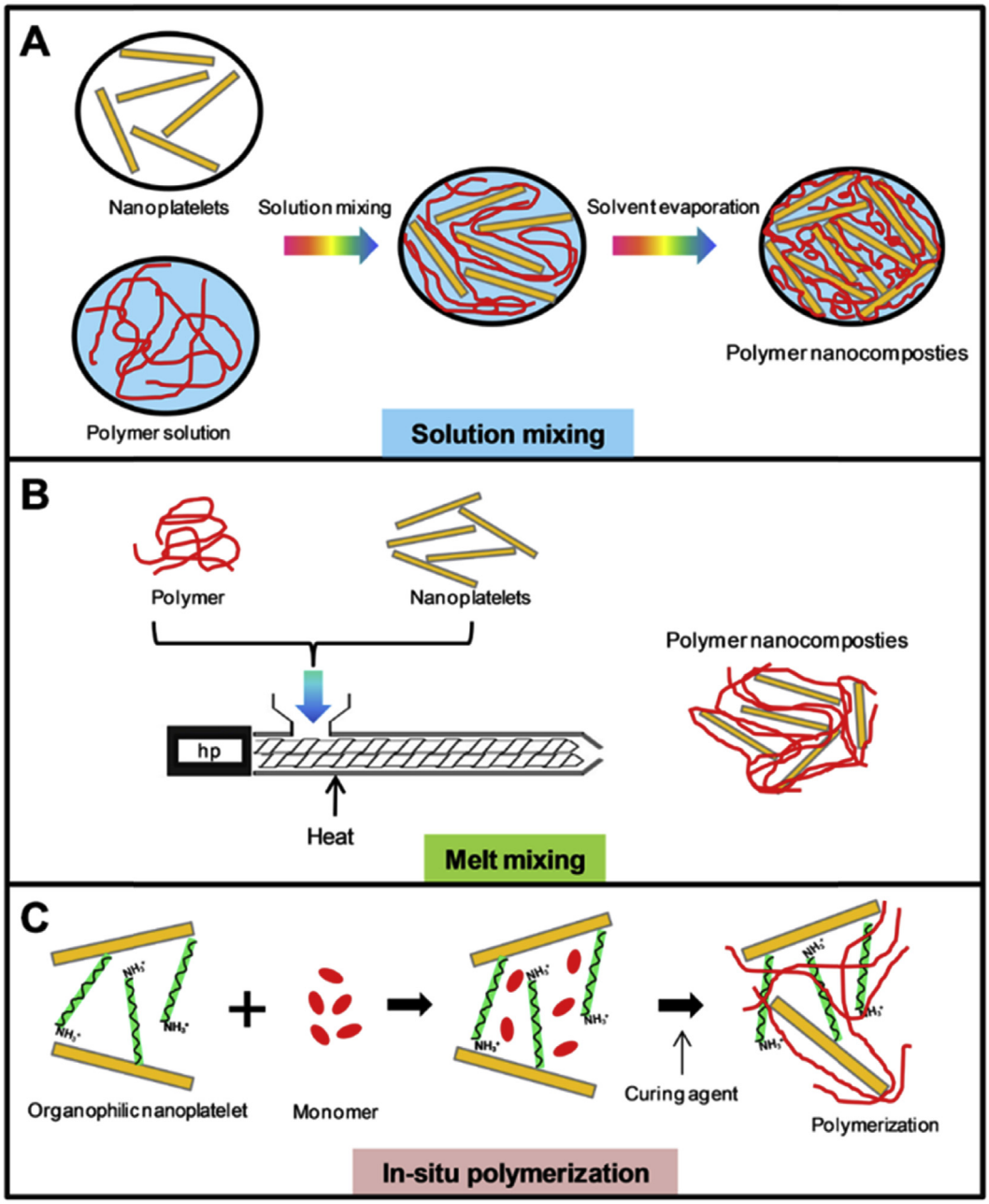

Fig. 3. Representative traditional methods for fabricating polymer nanocomposites. (A) The process of solution mixing includes two stages: solution mixing and solvent evaporation. (B) Melting mixing is a method of stirring the polymer and nanoplatelets above viscous flow temperature of polymer. (C) In-situ polymerization is mixture of monomer and nanoplatelets, and then polymerization forming TPNs.

adding 1.0 wt % of F-SWNTs. Stankovich et al. [24] demonstrated this simple approach for preparing graphene-based nanocomposites. The phenyl isocyanate-treated GO nanosheets were mixed with polystyrene (PS) in solvent of *N, N*-dimethylformamide. After removing the solvent, the GO-PS nanocomposites were further reduced by *N, N*-dimethylhylhydrazine to rGO-PS nanocomposites. This kind of rGO-PS nanocomposites exhibit a percolation threshold of 0.1 vol% for room-temperature electrical conductivity of 0.1 S/m.

However, there is a bottleneck problem in this process of solution mixing. The nanofillers could not be homogenously dispersed in solvent when increasing its content through simple mechanical mixing, resulting in aggregation of nanofillers. Then, the physicochemical properties of the resultant nanocomposites would decrease. To make the well-dispersion of nanofillers with high content, new ultrasound assisted solution mixing is developed for fabricating polymer nanocomposites. For instance, Jang et al. [47] dissolved the liquid crystalline epoxy resin (LCE), curing agent, and CNTs in acetone, then ultrasonicated for 1 h to obtain homogeneous mixing solution. Then the nanocomposites of CNTs-LCE are obtained after curing through removing acetone. With increasing of CNTs contents, the Young's modulus of CNTs-LCE nanocomposites was greatly enhanced at the same curing temperature.

Although the solution mixing is demonstrated to be a simple and effective way for fabricating TPNs in the past decades, however, several intrinsic bottleneck problems cannot be solved, including: i) high content of nanofillers in final nanocomposites are usually lower than 30 wt%; ii) the alignment direction is very difficult to be achieved in the process of solvent mixing; iii) the large quantity solvent utilized results environment damage [48]. Thus, the application of solution mixing is limited in scale-up production of TPNs.

2.1.2. Melting mixing

Melt mixing as a commercially attractive process is an alternative way for solving some issues of solution mixing [49]. The nanofillers are mechanically blended into thermoplastic matrix at a temperature above the viscous flow by a mixer, as shown Fig. 3B. Compared with solution mixing, the melting mixing usually is easily improving the content of nanofillers in the thermoplastic matrix, and there is no solvent environmental damage. For example, Kalaitzidou et al. [44] fabricated exfoliated graphite nanoplatelets (GN) reinforced polypropylene (PP). The resultant GN-PP nanocomposites showed high content GN of 10 vol%, and achieve 8% and 60% improvement in tensile strength and Young's modulus, respectively. Although many TPNs have been successfully fabricated by the melt mixing, it still remains several drawbacks, such as weak interfacial interactions between nanofillers and thermoplastic matrix, aggregation tendency due to the high surface energy, and the high viscosity of thermoplastic matrix, which are against the fine dispersion of nanofillers. Thus, ultrasonic approach is also used in melt mixing for preparation of TPNs, facilitating dispersion of nanofillers [50]. For instance, Lee et al. [51] prepared nanoclay reinforced-PP nanocomposites by melt mixing with the aid of ultrasonic. The exfoliation and dispersion of nanoclay are well achieved in the PP matrix. If nanofillers disperse in solution before melt mixing, the agglomeration of nanofillers in thermoplastic matrix could be reduced to some extent [52]. However, some thermoplastic matrices can be degradation above viscous flow temperature, which seriously affects the final performances [48]. In addition, the content of nanofillers is also limited due to the viscosity of thermoplastic and the alignment of nanofillers is very difficult to be achieved in the process of melting process.

2.1.3. In-situ polymerization

The in-situ polymerization is developed for achieving well dispersion of nanofillers in polymer matrix. First, the nanofillers disperse into the monomers or pre-polymers, and then polymerization proceeds by adjusting temperature [7,49], as shown in Fig. 3C. Besides the uniform dispersion of nanofillers in polymer matrix, the in-situ polymerization also provides opportunity for designing the different interfacial interactions between nanofiller and polymer matrix and avoids the degradation of polymer matrix [27].

For example, Trujillo et al. [53] demonstrated several kinds of CNTs reinforced high-density polyethylene (HDPE) by in-situ polymerization, and found an outstanding nucleating effect of CNTs regardless of the CNTs type. Kwon et al. [54] fabricated nitric acid treated multi-walled carbon nanotube (A-MWNTs)-waterborne polyurethane (PU) nanocomposites *via* in-situ polymerization. Results showed little content of A-MWNTs (1.5%) dramatically enhance the Young's modulus of A-MWNTs-PU nanocomposites. In order to further enhance the dispersion of nanofillers and interfacial interactions between monomers and nanofillers, surface modification of nanofillers is used in the process of in-situ polymerization. For example, Ma et al. [55] fabricated $CaCO_3$ reinforced poly (methyl methacrylate) (PMMA) nanocomposites. The results suggested that the surface modification of $CaCO_3$ by oleic acid improved the compatibility of $CaCO_3$ component and monomers, which promoted encapsulation of $CaCO_3$ in the PMMA. The approach of in-situ polymerization is suitable for preparing polymer nanocomposites whose polymer is insolubility or thermal instability [56]. However, with adding content of nanofillers, the viscosity is increasing, resulting in difficulty in manipulating [48]. Thus, the content of nanofillers is also relatively low in resultant polymer nanocomposites [27], which hinder the further improvement of the polymer nanocomposites performances.

2.1.4. Other methods

Besides above three procedures, there are many other methods used to fabricate TPNs such as emulsion polymerization [27], solid-state mechanochemical pulverization [57], high-shear mixing [46]. For example, emulsion polymerization is a common method for preparation of TPNs, such as PMMA, PS, and poly (styrene-acrylonitrite) (PSA) nanocomposites. Emulsion polymerization is usually utilized to prepare TPNs to obtain good dispersion of nanofillers with low viscosity [27]. Solid-state mechanochemical pulverization method is widely used to fabricate polymer nanocomposites, which needs to increase the viscosity of polymer to solid state, rather than avoids the high viscosity of polymer [57]. High-shear mixing could disrupt the nanofillers aggregates and realize homogenous dispersion in the polymer matrix [46]. However, these aforementioned methods can realize dispersion at low content of nanofiller in TPNs, and not form ordered structure.

On the other hand, some typical approaches for fabricating carbon fiber reinforced polymer composites are also introduced to prepare the nanocomposites, such as prepreg, resin transfer molding. For example, Wang et al. [58] first assembled the single-walled carbon nanotubes (SWNTs) into buckypaper *via* vacuum-assisted filtration, then infiltrated the solution of epoxy into the SWNTs buckypaper. The high content of SWNTs was achieved about 39 wt %, resulting in the high storage modulus with 15 GPa. Enrique et al. [59] fabricated CNTs-epoxy nanocomposites *via* infiltrating epoxy solution into aligned CNTs arrays. Although the volume fraction of CNTs is only about 2%, the Young's modulus have been improved to 11.8 GPa, corresponding to 220% increase compared to pure epoxy resin. To further improve the content of CNTs in the final nanocomposites, the mechanical densification is applied before infiltrating the epoxy resin [60], then the CNTs content

reaches as high as 20%. On the other hand, Ci et al. [61] synthesized the millimeter-long aligned MWNTs arrays *via* CVD process, and then infiltrated the liquid-state polydimethylsiloxane (PDMS) premixture with vacuum assistance. Finally, the continuous MWNTs-PDMS nanocompisites with about 5% volume fractions of MWNTs were achieved after curing. This continuous MWNTs-PDMS nanocomposite generated more than an order of magnitude enhancement in the longitudinal modulus with about 3300% under compressive loadings. Recently, the CNTs arrays are applied for preparing buckypaper *via* called “domino pushing” approach [19]. Cheng et al. [62] demonstrated CNTs-epoxy nanocomposite with vacuum-assisted resin infiltration approach. Continuous aligned CNTs were assembled into preform, which was infiltrated by epoxy resin. Furthermore, the content of CNTs in the resultant nanocomposites can be improved compared to aforementioned mixing procedures, for example, the content of CNTs was 8.13 wt% in the resultant nanocomposites. To further improve the content of aligned CNTs in the nanocomposites, the resin transfer molding was applied [63]. The content aligned CNTs reached as high as 16.5 wt%. The Young's modulus and tensile strength of aligned CNTs-epoxy nanocomposites reached 20.4 GPa and 231.5 MPa, respectively. These investigations indicated that much higher improvement of tensile strength and Young's modulus would be obtained with the same content of aligned CNTs than randomly CNTs.

Recently, the CNTs non-woven fabrics were continuously synthesized *via* floating catalytic chemical vapor deposition process [64,65]. Cheng et al. [66] applied prepregging approach to prepare the nanocomposites. First this random MWNTs fabric was aligned *via* stretching, and infiltrated by the bismaleimide (BMI) matrix, then the MWNTs-BMI nanocomposites were obtained after curing. The MWNTs content is up to ~60 wt %, and the tensile strength and Young's modulus reached up to 2088 MPa and 169 GPa along the MWNTs direction, respectively. After covalently cross-linking between MWNTs and BMI matrix [67], the tensile strength and Young's modulus of MWNTs-BMI nanocomposites are dramatically improved to 3081 MPa and 350 GPa along the MWNTs direction, respectively. However, these high mechanical properties are unidirectional performance, restricting the applications of these CNTs-based nanocomposites. Meanwhile, it is very difficult to realize the aligned structure for other nanofillers by the aforementioned traditional methods, such as MMT, graphene.

Therefore, the polymer nanocomposites prepared by above traditional methods still remain these drawbacks as following: 1) poor dispersion, 2) random structure, 3) low content of nanofillers, 4) weak interface, seriously limiting the improvement in physico-chemical properties of TPNs. In order to preparing high performance polymer nanocomposites, the novel concepts and approaches needed to be developed.

2.2. Bioinspired approaches

Nacre composed of inorganic and organic components shows extraordinary mechanical toughness, which is attributed to “brick-and-mortar” hierarchical micro/nano-scale structure and abundant interface interactions [68]. Thus, nacre provides a golden template for constructing BPNs. Several representative approaches for preparing BPNs are illustrated in Fig. 4, such as layer-by-layer [69],

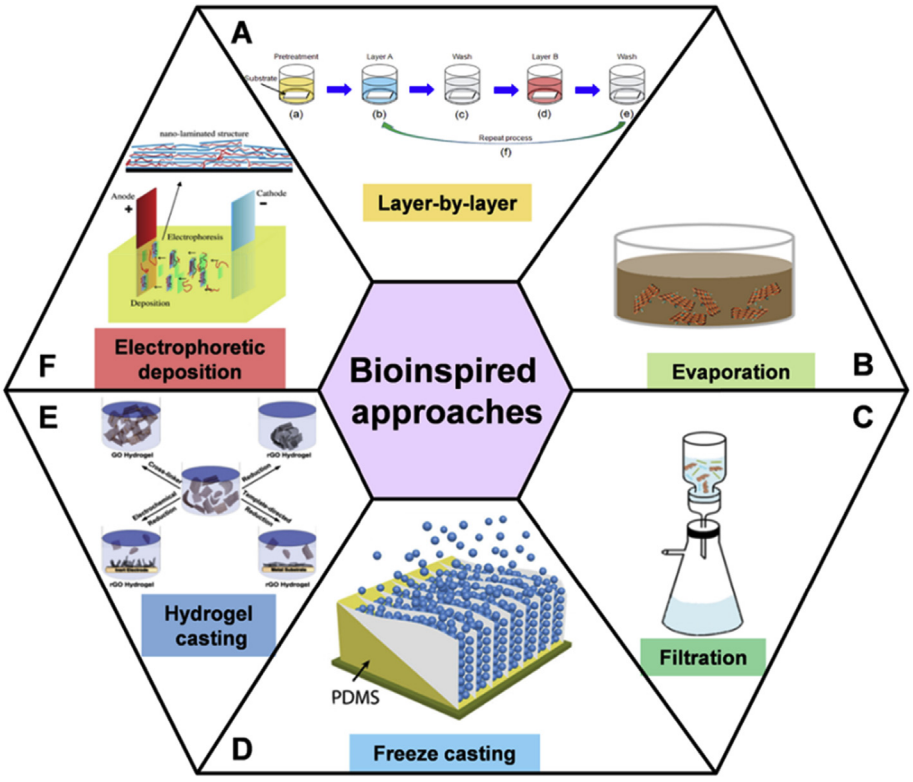

Fig. 4. Bioinspired approaches for constructing polymer nanocomposites. (A) Layer-by-layer could precisely control the structure of BPNs. However, it is difficult to scale up BPNs. (B) Evaporation is an easy operation to fabricate and scale up BPNs. However, time-consuming is the biggest issue of evaporation. Reproduced with permission [88]. (C) Filtration could form well layered structure, which is the most common method in our group. While, it is suitable for preparing thin films only. Reproduced with permission [93]. (D) Freeze casting is a new method that is more suitable for fabricating bulk composites with brick-and-mortar structure. Reproduced with permission [102]. (E) Hydrogel casting is fast and economical approach for BPNs, but, it is difficult to control the layered structure. Reproduced with permission [72]. (F) Electrophoretic deposition is simple for thin films. However, the resultant BPNs show relatively low mechanical performances. Reproduced with permission [108].

evaporation [26], filtration [70], freeze casting [71], hydrogel casting [72] and electrophoretic deposition [73]. These methods can realize a homogeneous dispersion, well-ordered alignment and interfacial interactions in the BPNs [74]. In the next sections, these bioinspired approaches will be discussed in details.

2.2.1. Layer-by-layer

Since 1991, Decher et al. proposed layer-by-layer (LBL) for forming multilayer films by alternately depositing polyelectrolytes with opposite charges at the liquid-solid interface based on electrostatic attraction mechanism [75,76]. LBL shows an advantage in fabricating layer and functional thin films with controllable size, component and morphology, which show unique optical, electrical and chemical properties. These thin films are widely used in microelectronic devices, wear-resistant layer and other technique fields [77,78]. Subsequently, LBL is also developed for preparing thin films upon varying driving forces, such as hydrogen bonding [79], molecular recognition [80], coordination bonding [81] and surface gelation process [82]. The process of layer-by-layer assembly technology is described as following [39] in Fig. 4A: (a) Substrate should be pretreated including wash and surface treatment; (b) A layer film is absorbed onto the substrate upon driving forces; (c) The substrate with A layer is washed before absorption of B layer film, which avoid pollution and make the layered structure stability; (d) The substrate is immersed into B solution and B layer film is absorbed on the A layer film based on driving forces; (e) the substrate with A and B layers was washed again, (f) Recycle the process of (b) (c) (d) (e). The LBL is a versatile and prevalent approach for preparing desired multilayer films. For example, Kleinfeld et al. [83] firstly demonstrated multilayered structure nanocomposites *via* assembling positively charged polydiallydimethylammonium chloride (PDDA) and anionic MMT nanosheets through layer-by-layer technique. Then the strong interfacial interactions are constructed in the process of LBL technique, resulting in high performance BPNs. Tang et al. [84] prepared nanoclays-polyelectrolytes multilayers nanocomposites with tensile strength comparable to nacre and Young's modulus similar to lamellar bones. The results revealed that the outstanding mechanical properties were not only determined by the ordered brick-and-mortar hierarchical structure, but also the ionic crosslinking of tightly folds macromolecules with the saw-tooth pattern of stretching curves. Modification surface of building blocks is an important means for enhancing the interfacial interactions between the polymer matrix and building blocks. For instance, Bonderer et al. [85] prepared amine-modified alumina (Al_2O_3)-chitosan (CS) films with brick-and-mortar structure by assembly at the air-water interface and spin-coating. The work fracture of resultant films is one order of magnitude of natural nacre. Podsiadlo et al. [39] demonstrated ultrastrong and stiff BPNs based on nanoclay and PVA *v*ia LBL technique. The MMT-PVA nanocomposites after glutaraldehyde (GA) crosslinking exhibit high strength of 400 MPa, and recorded Young's modulus of 107 GPa, respectively. Recently, Xiong et al. [86] prepared high performance rGO-cellulose nanocrystals nanocomposites with high tensile strength of 655 MPa and Young's modulus of 169 GPa. To sum up, the LBL technique shows many advantages for preparing BPNs, such as precise control of hierarchical structure and high content of building blocks, however, several issues including scaling up and time-consuming should be solved before application in the industrial filed for fabricating BPNs.

2.2.2. Evaporation

Compared with LBL technique, a simple and easy operation process of evaporation has been developed for preparing BPNs in the lab. Evaporation could be utilized for mimicking the nano ordered structure of organic-inorganic hybrid materials in nature. In the process of evaporation, the nanosheets in the solution tend to be arranged in a low energy structure with the removal of solvent, thus forming layered ordered structure. For example, Walther et al. [87] fabricated nacre-like MMT-sodium carboxymethyl cellulose (CMC) BPNs by evaporation. The resulted BPNs showed extraordinary mechanical properties. The stiffness and strength are 25 GPa and 320 MPa, respectively. Cui et al. [88] fabricated bioinspired layered nanocomposites of GO-polydoamine (PDA) by evaporation-induced assembly. The tensile strength and toughness of GO-PDA exhibited 1.5 and 2 folds higher than that of nacre, which are attributed to layered hierarchical structure and covalent bonding between GO nanosheets and PDA molecules. The evaporation process can also be utilized for preparing ternary BPNs. For example, Morits et al. [89] presented the aligned bulk high-performance MMT-PVA nanocomposites with centimeter thickness. Wang et al. [33] prepared MMT-nanofibrillar (NFC)-PVAnanocomposites, and the mechanical properties exceed that of nacre and conventional layered MMT-polymer binary nanocomposite. Although the higher temperature could accelerate the evaporation, it is not conducive to the formation of an orderly structure. In addition, it is really difficult to achieve well layered structure of BPNs, and usually takes long time for evaporating the solvent in the fabrication process.

2.2.3. Filtration

Similar to evaporation, the filtration is another simple and effective method for preparing BPNs [74,90], as shown in Fig. 4C. In the process of filtration assisted with vacuum, nanosheets in the suspension could be deposited on the surface of filter and arranged to form an ordered layered structure with the flow of solvent.

For example, Walther et al. [91,92] used a colloidal self-assembly of core-shell hard/soft polymer-coated nanoclay into a highly ordered layered structure of nacre-mimetics by vacuum filtration induced self-assembly, which showed very good mechanical properties as well as the fire barrier properties. Wang et al. [70] prepared layered MMT-poly (N-isopropylacrylamide) (PNIPAM) nanocomposite hydrogel (L-NC) by vacuum-assisted filtration. Compared with randomly MMT-PNIPAM nanocomposite hydrogel (R-NC), the strength and toughness of L-NC with high nanoclay content are much higher than that of R-NC. Wan et al. [93] demonstrated GO-polyacrylic acid (PAA) nanocomposites with high tensile strength and toughness by vacuum-assisted filtration and investigated the effect of environmental relative humidity on the GO-PAA. Vacuum filtration was also applied to assemble the high performances of GO-molybdenum disulfide (MoS_2)-thermoplastic polyurethane (TPU) [94], GO-DWCNT-PCDO [95], and GO-DWCNT-PVA [96] ternary BPNs. The limitation for filtration approach is the size of filtration setup and filtration speed, resulting in the difficulty in scaling up.

2.2.4. Freeze casting

In sea water, there are salt, biological organisms, etc. but ice can form a matrix of crystals when water contains impurities and the impurities could be expelled into the interstices of the ice [97,98]. Inspired by this phenomenon, the novel ice templating freeze casting technique is developed, as shown in Fig. 4D. The mechanism of freeze casting is the growing ice forms lamellar microstructures during freezing and layered, uniform ceramic scaffold, a negative replica of ice, is formed by ceramic particles concentrating in the gap of the ice [98]. It is a molding technique used to cast complex structure. Since the developed in 2006, freeze casting has been used for preparation of porous ceramic materials [98,99]. It is a novel environmentally friendly and inexpensive techniques for constructing bulk BPNs [100,101]. For example, Deville et al. [98] first developed ice-templating method to assemble sophisticated

porous and layered-hybrid materials, such as artificial bone, nacre-like ceramic composites, and porous scaffolds for osseous tissue regeneration. Munch et al. [71] further applied the ice-templating to mimicking the nacre structure by combing two ordinary compounds, Al_2O_3 and PMMA into nacre-like ceramic materials, which shows the superior toughness over 300 times than that of constituents, and high yield strength and fracture toughness. Recently, a new bidirectional freezing technique has been demonstrated for scaling up fabrication of layered scaffold based on ice-templated approach [102].

Although the great progress has been achieved by using ice-templated approach in mimicking nacre-like nanocomposites, the precise structure of nacre is still very difficult to be replicated by the ice-templated approach. For example, the scaffolds show relatively low inorganic volume fractions, require high temperature sintering. Recently, Mao et al. [103] developed a novel ice-template approach by alternatively freezing water-soluble orgainc molecules into scaffold, then the mineralization would process in the organic scaffold. This modified ice-template approach demonstrates several advantages, such as high inorganic fraction, ambient mineralization, and assembling heat-labile materials.

2.2.5. Hydrogel casting

Hydrogel casting is also a fast, effective, economical approach for preparing BPNs [104], especially for the GO-based BPNs [105]. GO nanosheets with hydrophilic and hydrophobic groups on its surface can swell in water and easily assemble into 3D network structure. If the organic crosslinking agent is introduced in the preparation of GO hydrogel, the BPNs can be fabricated by hydrogel casting. Moreover, GO based hydrogels show low critical gelation concentration and excellent reversibility upon chemical stimulations [104]. The interactions of GO nanosheets promoted to form the gelation of GO including hydrogen bonding, π-π stacking, electrostatic interaction and coordination [104,105]. The strategy for preparing GO and rGO hydrogels is shown in Fig. 4E. Hydrogel casting is a simple and feasible approach for preparing flexible large-area hierarchical BPNs through different interfacial interactions [72,104]. For example, the GO-poly(acrylic acid-*co*-(4-acrylamidophenyl)boronic acid) ($PAPB_x$) nanocomposites with trace amounts of $PAPB_x$ show great improvement in mechanical properties than pure GO film. The ultralow critical gelation concentrations (cgc) (<1 wt %) of $PAPB_x$ facilities the GO to form hydrogels. The delicate hydrophobic-hydrophilic balance, modulated by $PAPB_x$ for the formation of homogeneous GO-$PAPB_x$ hydrogels, improves the mechanical properties of GO-$PAPB_x$ nanocomposites [106]. However, it remains great challenges for precisely controlling the laminated structures and designable interfacial interactions.

2.2.6. Electrophoretic deposition

Electrophoretic deposition has attracted much attention because of its short time-consuming, low cost and controllability. As a general technique, it has been widely used in the ceramic and colloidal process. Nowadays, it is also suitable for fabricating thin BPNs with well laminated structures [74,107], as shown in Fig. 4F. For example, the typical electrophoretic deposition process involves the following two steps: the charged particles are first moved to the oppositely charged electrode under the action of an electric field, and then form a thin film on the surface of an electrode. For instance, Long et al. [73] modified MMT nanosheets by acrylamide monomers in an aqueous suspension, and then deposited the modified MMT nanosheets on the electrode. Under ultraviolet-radiation, the acrylamide modified MMT nanosheets polymerized into MMT-polyacrylamide (PAM) nacre-like nanocomposite with brick-and-mortar structure and high hardness of 0.95 GPa, and Young's modulus of 16.92 GPa. Lin et al. [107] reported a facile electrodeposition method to prepare large-area polymer nanocomposites with layered structures. Lin et al. [108] demonstrated MMT-acrylic anodic electrophoretic resin (AAER) nanocomposites by special hydrothermal-electrophoretic assembly which can control the nanostructure and organic content. Similarly, the electrophoretic deposition process is also difficult to prepare large area and thick BPNs because of the limitations of setup [74].

The abovementioned six approaches are typical strategies for preparing BPNs with hierarchical structures and high content of building blocks. Compared with TPNs prepared by traditional methods, BPNs show higher mechanical properties that attribute to well dispersion, alignment structure and high content of building blocks. In fact, the interfacial interactions between building blocks and polymers also play a critical role in improving mechanical properties of polymer nanocomposites, especially for BPNs. We would introduce the importance of interfacial interactions design in polymer nanocomposites in the following sections. The advantages and disadvantages of traditional methods for TPNs and bioinspired approaches for BPNs are listed in Table 1.

3. Interfacial interactions design

Due to the fact that numerous nanofillers are inert materials, such as CNTs, they do not improve or even decrease the mechanical performances of TPNs. To solve the issues above, several typical approaches have been developed for dispersing nanofillers into polymer matrix, such as surface grafting and coupling reaction, surfactant adsorption, polymer wrapping, as shown in Fig. 5. Surface grafting is an effective way of modifying the surface of nanofillers, as shown in Fig. 5A. Some functional groups are introduced into insert surface nanofillers, which facilitate the chemical covalent bonding with matrix. For example, Wang et al. [109] grafted the epoxy curing agent to the SWNTs through diazotization, and achieved a uniform SWNTs dispersed epoxy nanocomposites. The Young's modulus of resultant nanocomposites was improved 24.6% with only 0.5 wt% content of functionalized SWNTs.

Table 1
Comparison of traditional methods for preparing TPNs and bioinspired approaches for fabricating BPNs.

Methods		Advantages	Disadvantages
Traditional methods	Solution mixing	Simple	Environment damage
	Melt mixing	Without solution	Uneven dispersion
	In-situ polymerization	Uniform dispersion	Difficult to manipulate
Bioinspired approaches	Layer-by-layer	Precise control of layered structure	Time-consuming
	Evaporation	Easy operation	Difficult to precisely control alternative layered structure
	Filtration	Easy to operation	Difficult to scale up
	Freeze casting	Bulk materials	Energy-consuming
	Hydrogel casting	Economical, large-scale size	Difficult to control the layered structure
	Electrophoretic deposition	Precisely controllability	Difficult to prepare thick film

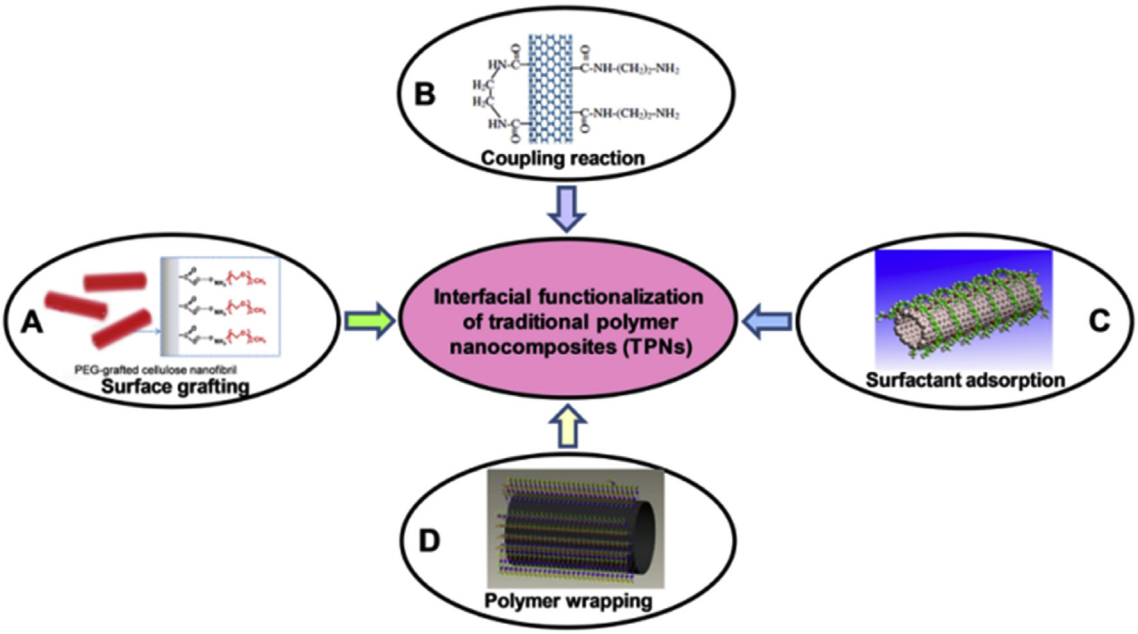

Fig. 5. Interfacial functionalization design for TPNs, which could be divided into two classies. i) Covalent functionalization (A) Surface grafting. Reproduced with permission [109]. (B) Coupling reaction. Reproduced with permission [111]. The drawbacks of covalent functionalization could destroy the original structure of nanofillers. Non-covalent functionalization could solve the issues above, such as(C) Surfactant adsorption. Reproduced with permission [110]. (D) Polymer wrapping. Reproduced with permission [110].

In addition, functionalization of CNTs through coupling reaction was also developed. Organic amine was directly coupled with carboxylic groups on the surface of CNTs. The amino-functionalized CNTs showed high surface energy and wettability with epoxy resin, which inhibited the aggregation of CNTs and improved the mechanical properties of epoxy compared with pristine CNTs [110], as shown in Fig. 5B. The aforementioned two types of surface modification are covalent method [111]. The defects in building blocks are usually introduced, which may seriously affect the performance of intrinsic nanofillers such as mechanical and electrical properties. Thus, non-covalent functionalization is an alternative method to modify the surface of nanofillers and improve the interfacial interactions of polymer nanocomposites compared with covalent functionalization [38]. As shown in Fig. 5C, surfactant adsorption has been utilized to functionalize the surface of nanofillers to realize well dispersion in polymer matrix [110]. Many studies have been confirmed the effects of surfactant such as polyoxyethylene 8 lauryl, poly (styrene sulfate), dodecyl tri-methyl ammoniumbromide [27]. On the other hand, polymer wrapping is also developed to factionalize the nanofillers by interfacial interactions such as the van der Waals and π-π stacking, which could modify and tune the interfacial properties of nanofillers [110], as shown in Fig. 5D. For example, the CNTs are wrapped in polystyrene (PS) to form supermolecular complexes, which contribute to realize uniform dispersion of CNTs into the polymer matrix [110,111].

Although the physicochemical properties of TPNs have been improved in some extent *via* aforementioned methods, it still remains a great challenge for achieving the high performance polymer nanocomposites as theoretically expected [30]. For BPNs, the abundant interfacial interactions play a key role in improving the mechanical properties [112]. Based on the studies of our and other groups, various interfacial interactions in BPNs have been developed and categorized into i) non-covalent bonding, including hydrogen bonding, ionic bonding and π-π interaction, ii) covalent bonding, containing linear molecule and polymer, branched polymer, 3D network, as shown in Fig. 6. In the following sections, we summarize recent studies of our group and others on the interfacial designs of BPNs in details.

3.1. Non-covalent bonding

The interfacial interactions play a critical role in the properties of BPNs. Common non-covalent bonding, such as hydrogen bonding, ionic bonding and π-π interactions, can enhance the mechanical performance of BPNs. Utilizing these different non-covalent bonding between the building blocks, researchers could tune the strength, strain resistance, toughness and fatigue of resultant BPNs.

3.1.1. Hydrogen bonding

Hydrogen bonding is one of the most common and most important intermolecular or intramolecular interactions [40]. Although hydrogen bonding is a weak bond, it would have an impact on the aggregation state of matter because of its formation and significantly change the physical properties, shape and structure of matter [93]. Due to the abundant oxygen-containing functional groups on the surface of GO, hydrogen bonding is ubiquitous in BPNs. Walther et al. [113] has constructed the interfacial interactions based on hydrogen bonding between polymer and nanoclay and demonstrated the effects of aspect ratio of nanoclays on structural, mechanical and functional properties. Dikin et al. [114] first prepared GO film with ordered layered structure by filtration. Because of the hydrogen bonding between GO and H_2O, the GO paper shows excellent mechanical properties, tensile strength of 133 MPa and Young's modulus of 32 GPa. Besides water molecules, polymers could also form rich hydrogen bonding with GO nanosheets, such as PAA, PVA. For example, PAA formed hydrogen bonding with GO nanosheets to improve the mechanical properties of GO-PAA BPNs [93], as shown in Fig. 7A. The tensile strength and toughness of rGO-PAA BPNs with PAA content of 4.51 wt% were 2 and 3.3 times than that of pure reduced GO film, respectively. Meanwhile, rGO-PAA BPNs showed high electrical conductivity of 108.9 S/cm. In addition, Wan et al. [93] also investigated the influence of environmental relative humidity on

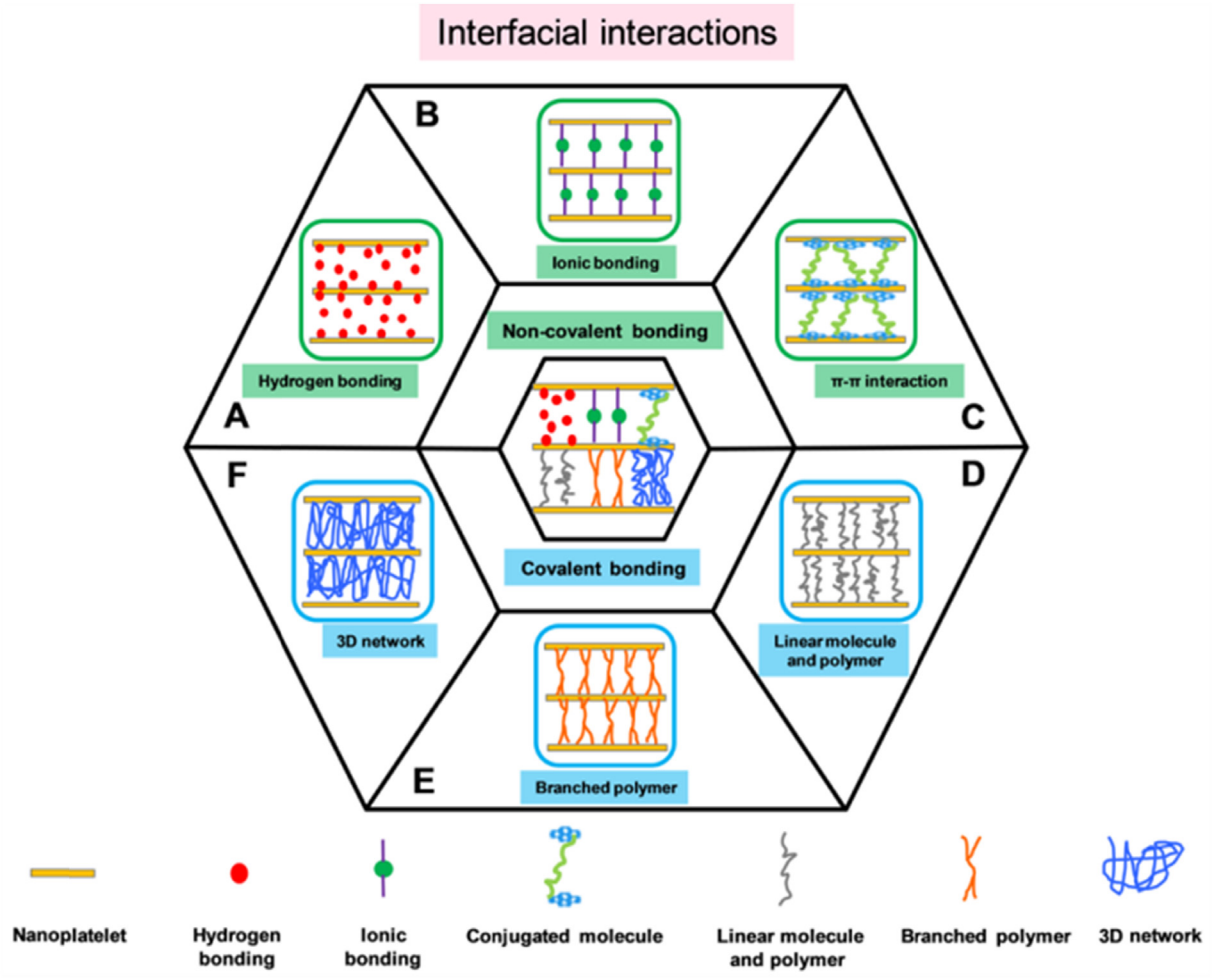

Fig. 6. Bioinspired strategy for constructing high performances of BPNs. Inspired by the hierarchical structure and abundant interfacial interactions of nacre, high properties of BPNs are prepared by various interfacial interactions that could be divided into two categories. Non-covalent bonding. (A) Hydrogen bonding. (B) Ionic bonding. (C) π-π bonding. And covalent bonding. (D) Linear molecule and polymer. (E) Branched polymer and (F) 3D network.

mechanical properties of rGO-PAA BPNs. With the increasing of humidity, the tensile strength and Young's modulus of GO, rGO, GO-PAA and rGO-PAA decrease. While the toughness of rGO-PAA showed no obvious decreasing because water served as lubricant rather than bridge between rGO nanosheets. PVA, a common polymer matrix with abundant hydroxyl, is also an ideal candidate for preparing GO-based BPNs. For instance, Li et al. [40] prepared GO-PVA BPNs with bricks-and-mortar structure like nacre, resulting in high mechanical performances that attributed to the formation of hydrogen bonding between GO and PVA when its loading was 20 wt%. The tensile strength and Young's modulus of GO-PVA were increased of 75.9% and 178%, respectively, compared with that of pure GO. Thus, the results above reveal that the formation of hydrogen bonding between GO and polymer could dramatically enhance the mechanical properties of BPNs, creating a guidance for constructing other layered BPNs.

3.1.2. Ionic bonding

The study of protein structure of biomaterials found that trace amount of metal ions can greatly improve mechanical performances [74]. The GO nanosheets with abundant oxygen-containing functional groups are favorable for the coordination of metal ions. Since 2008, Park et al. [41] first fabricated GO-Mg^{2+} and GO-Ca^{2+} films with less than 1 wt% of Mg^{2+} and Ca^{2+}. The results showed that Mg^{2+} and Ca^{2+} could significantly improve the mechanical performances of GO film by formation of ionic bonding between adjacent GO nanosheets. In addition, it was also found that the tensile strength and Young's modulus of GO-Mg^{2+} were 87.9 MPa and 24.6 GPa, respectively, which were higher than those of GO-Ca^{2+} (the tensile strength of 75.4 MPa, the Young's modulus of 21.5 GPa), because the fact ionic radius of Mg^{2+} is lower than Ca^{2+} (Fig. 7B). Yeh et al. [115] discovered that GO films could be stable in water by filtration using anodized aluminum oxide (AAO) filter discs, which was contradictory with the electrostatic repulsion of GO nanosheets. Instead, the GO films would disperse when fabricated by infiltration using a Teflon filter membrane. The reason was that GO films prepared by AAO filter discs can be cross-linked by introducing trace amounts of Al^{3+} obtained from corroding of AAO. Furthermore, The tensile strength and Young's modulus of GO films (AAO) reached up to 100.5 MPa and 26.2 GPa, respectively, which were much higher than that of GO films (Teflon) (tensile strength of 86.9 MPa and Young's modulus of 7.6 ± 1.1 GPa). Walther et al. [116] studied the effects of divalent Cu^{2+} ionic supramolecular interaction on mechanical properties of MMT-CMC at different humidity. Such ionic crosslinking can preserve the mechanical properties at high humidity [117]. Recently, Chen et al. [118] demonstrated ionic bonding between 2D nanosheets, such as MMT, GO, can significantly improve mechanical properties of the resultant composites.

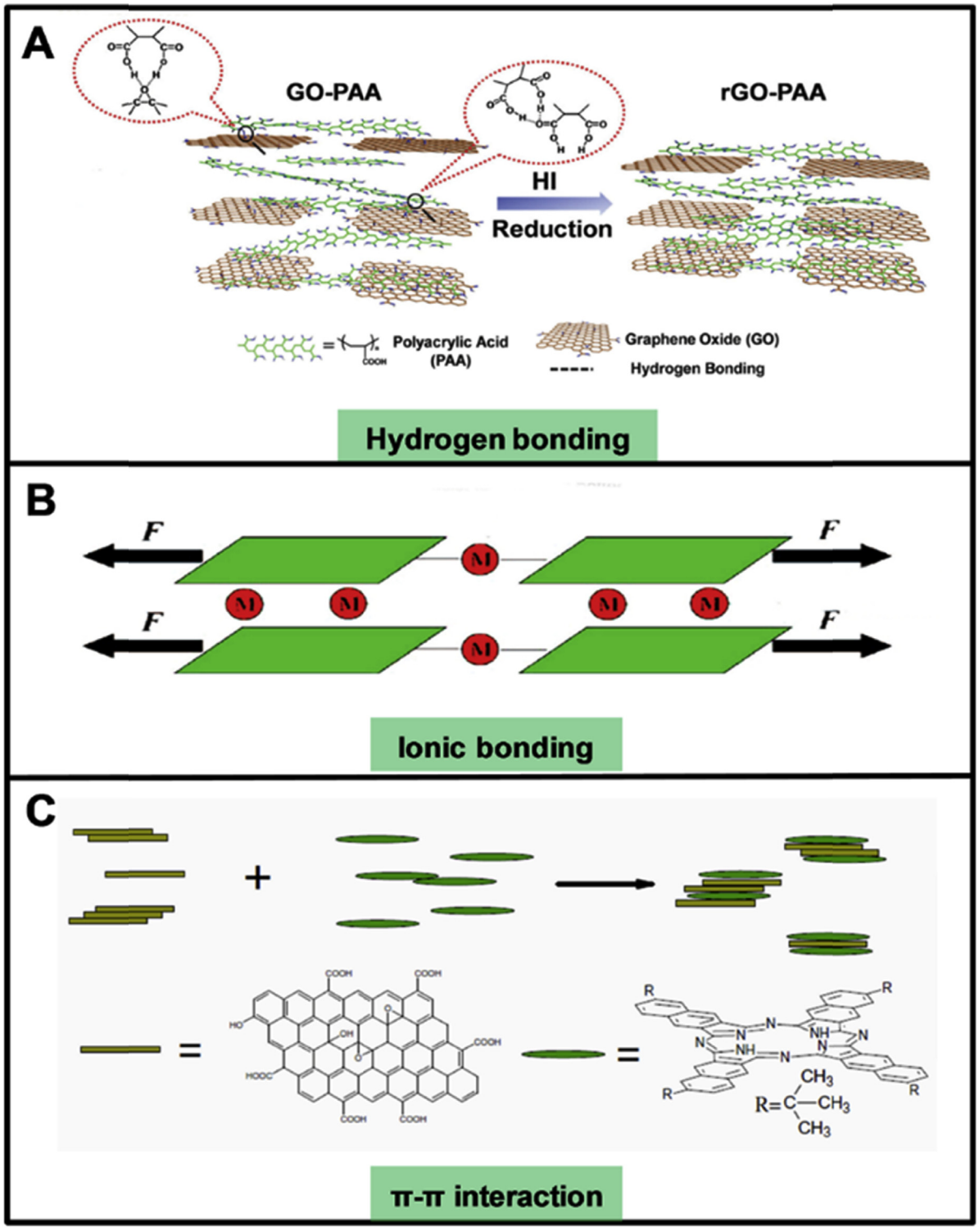

Fig. 7. Non-covalent bonding. (A) Hydrogen bonding between PAA and GO nanosheets could dramatically improve the mechanical properties of BPNs. Reproduced with permission [93]. (B) Ionic bonding between the adjacent GO nanosheets could enhance the external resistance. Reproduced with permission [41]. (C) GO-NPC by π-π interactions supermolecular method could be stable and utilized as photoelectric conversion devices. Reproduced with permission [119].

In contrast to the abovementioned single ion enhancement, this article presented metal ion synergic cross-linking strategy by using eight types of metal ions, such as Mg^{2+}, Zr^{2+}, Ni^{2+}, Al^{3+}. The results presented synergic metal ions can dramatically enhance the mechanical properties of resultant nanocomposites.

3.1.3. π-π interaction

It is well known that there is strong π-π interaction in graphite, resulting in its stability. With similar principle, graphene with SP^2 hybrid structure could be utilized for constructing BPNs with conjugated molecules or polymer *via* π-π interaction. For example,

Zhang et al. [106] fabricated $PAPB_x$ through introducing phenylboronic acid moieties into PAA. A small amount of PAPBx (less than 1 wt %) could lead to the formation of hydrogels with GO, enhencing π-π interactions with GO nanosheets. The tensile strength and toughness of rGO-$PAPB_x$ reached up to 382 MPa and 7.5 MJ m^{-3} with 4 wt % of $PAPB_x$, respectively. Meanwhile, the wrinkles of GO nanosheets increased interfacial area and thus enhanced the mechanical properties of rGO-$PAPB_x$. The strong π-π interaction between GO and polymer is not only utilized for reinforcing mechanical performance, but employed in optoelectronic fields. For instance, Zhang et al. [119] prepared the layered GO-NPC (naphthalocyanine) BPNs by the π-π interactions supermolecular method. The π-π interactions were confirmed between GO and NPC through adsorption and fluorescence spectra analysis, resulting in GO-NPC stability under ambient condition. The GO-NPC BPNs can be used as efficient photoelectric conversion devices.

3.2. Covalent bonding

Although non-covalent bonding above dramatically improve the mechanical performance of BPNs, they can be destroyed easily in solution, salts and pH value [68]. In order to make BPNs work in harsh conditions, covalent bonding exhibiting greater robustness is employed to fabricate highly cooperative BPNs. Linear molecule and polymer, branched polymer and 3D network resin are utilized to construct covalent bonding in the BPNs, which would be described in details in the following sections.

3.2.1. Linear molecule and polymer

Linear molecule and polymer with reactive functional groups could react with GO nanosheets to form covalent bonding networks, which significantly improve the mechanical properties of BPNs. Recently, borate and GA, common linear molecules, are used for improving the mechanical properties of GO film by crosslinking GO nanosheets. For example, An et al. [120] constructed stiff layered GO-borate BPNs through borate crosslinking. The results showed that the tensile strength and storage modulus of GO film with only 0.94 wt % borate ions were improved 25% and 266%, respectively. Gao et al. [42] demonstrated GO-GA BPNs by crosslinking adjacent GO nanosheets with GA. The Young's modulus was ~30.4 GPa and the tensile strength was 101 MPa, which were much higher than GO film. However, short GA chains led to low toughness with only 0.3 MJ m^{-3}.

Besides linear molecules, long chains polymer such as 10,12-pentacosadiyn-1-ol (PCDO) was employed for preparing GO-PCDO BPNs, which overcome the issue of low toughness caused by short linear molecules. Cheng et al. [121] fabricated high integrated performances of GO-PCDO BPNs. The process of preparing GO-PCDO was divided into three steps: i) PCDO monomers reacted with GO nanosheets by esterification reaction; ii) PCDO monomers polymerized and partly cross-linked by UV irradiation crosslinking; iii) the resultant GO-PCDO BPNs was reduced by HI solution, removing the residual chemical groups of GO nanosheets, as shown in Fig. 8A. The tensile strength of rGO-PCDO reached up to 156.8 MPa, and the toughness was 3.91 MJ m^{-3}, which were much higher than that of pure rGO film. In addition, the electrical conductivity of rGO-PCDO showed as high as 232.29 S cm^{-1}.

3.2.2. Branched polymer

Branched polymer has been considered as cross-linker owing to

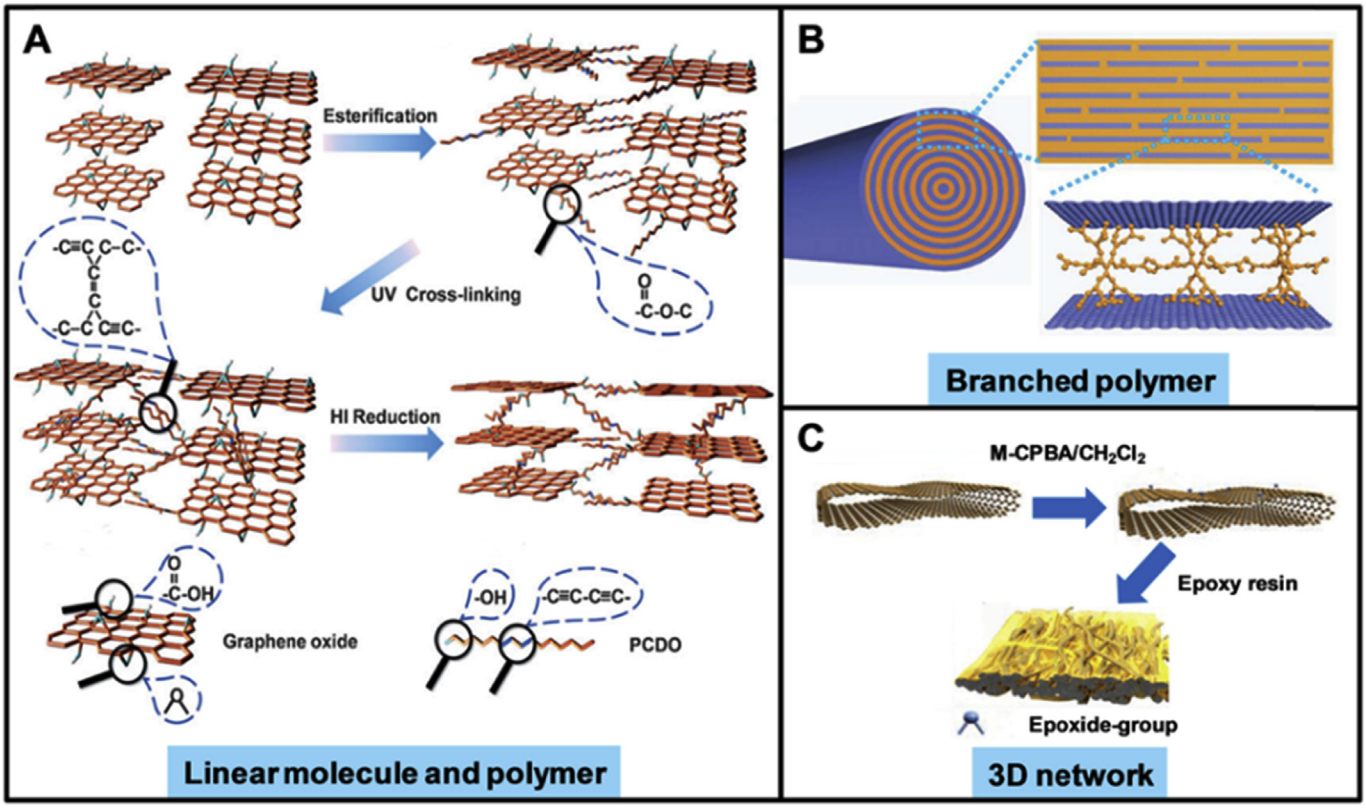

Fig. 8. Covalent bonding. (A) Linear molecule and polymer such as PCDO could enhance the performances of GO by forming covalent bonding. Reproduced with permission [121]. (B) Branched polymer with multiple sites could be employed for cross-linking with building blocks. Reproduced with permission [122] (C) Thermosetting matrix such as epoxy resin could react with GO nanosheets and form 3D network by self-polymerization, resulting in high mechanical performances BPNs. Reproduced with permission [32].

its multiple reactive functional group sites for improving the mechanical properties of BPNs. The hydperbranched polyglycerol (HPG) as representative branched polymer was selected to fabricate the BPNs. For example, Hu et al. [122] constructed GO-HPG fibers by forming covalent bonding between GO nanosheets and HPG, as shown in Fig. 8B. The tensile strength of GO-HPG fibers was improved to 642 MPa from 555 MPa for pure GO fiber. Until now, there are a few studies on the branched polymer cross-linked BPNs, which might be difficult to synthesize suitable branched polymers.

3.2.3. 3D network

Thermosetting polymer with reactive functional groups, such as epoxy, can graft on the surface of building blocks and cross-link adjacent building blocks *via* three dimensional (3D) network structure. For example, Cheng et al. [32] fabricated high performance FDWCNT-epoxy BPNs with high content of FDWCNT (70 wt %) and layered hierarchical nacre-like structure, as shown in Fig. 8C. The epoxy precursor reacted the epoxide groups on the surface of FDWCNTs and formed 3D network between adjacent FDWCNTs. The results showed that the highest Young's modulus of resultant FDWCNT-epoxy composites reaches 123 GPa, which was 6 times higher than pure epoxy. Graphene as one best of ideal candidates for preparing BPNs has been employed to fabricate cooperative graphene foam (GF)-epoxy BPNs by Ming et al. [123]. The GF-epoxy BPNs was prepared as follows: i) GF was obtained through GO films were reduced through $N_2H_4 \cdot H_2O$ vapor, ii) the GF was immersed the epoxy resin solution and iii) the GF-epoxy was prepared by the hot-pressure, realizing cross-linking. The tensile strength, Young's modulus and electrical conductivity of resultant BPNs were 23, 136 and 8 times of pure GF, respectively.

The aforementioned interfacial interactions could dramatically improve the mechanical properties and electrical conductivity of resultant BPNs. However, how to precisely control the interfacial interactions to prepare high performance BPNs is still great challenges.

4. Synergistic effects

Over billions of years, the extraordinary mechanical performances of natural materials are not only determined by the building block, biopolymers and interfacial interactions [124], but also partly attributed to the synergistic effects of interfacial interactions [125] or building blocks [23]. Thus, various BPNs were constructed with synergistic effects. The synergistic effects of BPNs can be divided into synergistic interfacial interactions and synergistic building blocks, as shown in Fig. 9. In the next sections, we

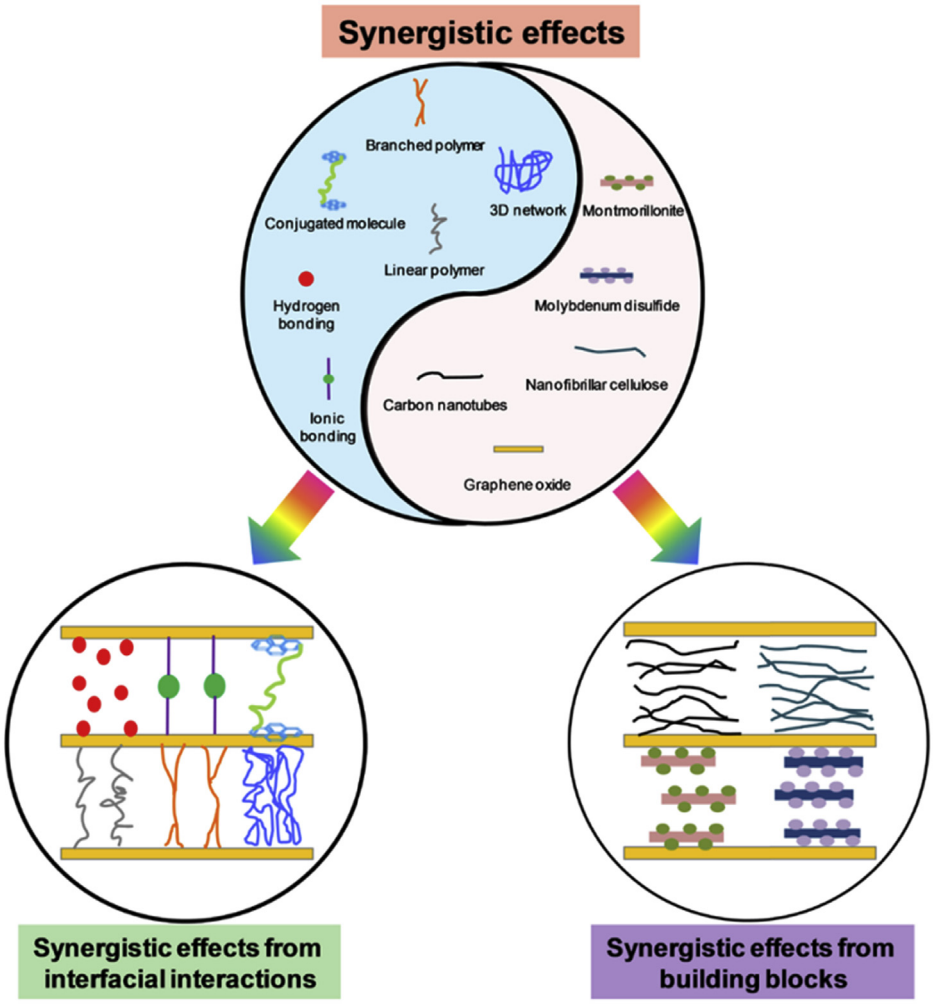

Fig. 9. BPNs are fabricated with different synergistic effects, including synergistic effects from interfacial interactions and synergistic effects from building blocks. Synergy from interfacial interactions includes hydrogen bonding and π-π interaction, hydrogen and ionic bonding, hydrogen and covalent bonding, ionic and covalent bonding. Synergy from building blocks consists of 1D and 2D building blocks.

would focus on these BPNs from our and other groups.

4.1. Synergistic effects from interfacial interactions

Hydrogen bonding, ionic bonding, π-π interaction and covalent bonding have been utilized to construct high performances GO-based BPNs by combing different interfacial interactions. Until now, four kinds of synergistic interfacial interactions have been demonstrated, which would be discussed in the next sections.

4.1.1. From hydrogen bonding and π-π interaction

Song et al. [126] has demonstrated the synergistic effects from hydrogen bonding and π-π interaction through triblock copolymer, and fabrication process is shown in Fig. 10A. Water-soluble sulfonated polystyrene-*block*-poly (ethylene-*co*-butylene)-*block*-polystyrene (SSEBS) triblock copolymers with sulfonic groups could form hydrogen bonding with oxygen-containing groups on the surface of GO nanosheets. The digital photograph of this GO-SSEBS BPNs is shown in Fig. 10B. Strong π-π interactions were formed between SSEBS and GO nanosheets due to the benzene groups of SSEBS. The resultant GO-SSEBS exhibited super-tough and further revealed that SSEBS can significantly improve the tensile strength and toughness of GO film *via* synergistic effects from hydrogen bonding and π-π interactions. The tensile strength and toughness of GO-SSEBS were 158 MPa and 15.3 MJ m^{-3}, respectively, which were 76% and 900% improvement than pure GO film and the toughness was 8 times than nacre when the content of SSEBS was about 10 wt%. The content of SSEBS played a critical role in the mechanical performances of GO-SSEBS, resulting in the tensile strength and toughness decreasing when the content of that lower or higher than 10 wt%, as shown in Fig. 10C. The fracture mechanism was proposed as follows. When gradual loading of GO-SSEBS, it firstly exhibited plastic deformation with soft long chains of SSEBS deformation and extending, dissipating much energy. Second, EB chains in SSEBS further extend to uncoil until rupture, as shown in Fig. 10D. Finally, GO nanosheets were pulled out and the GO-SSEBS fractured, as shown in Fig. 10D. Finally, GO nanosheets were pulled out and the GO-SSEBS fractured.

4.1.2. From hydrogen bonding and ionic bonding

Recently, synergy from hydrogen and ionic bonding is investigated by preparing GO- hydroxypropyl cellulose (HPC)-Cu^{2+} BPNs by Zhang et al. [127]. HPC could form hydrogen bonding with GO nanosheets. The Cu^{2+} was introduced in GO-HPC to work as ionic bonding and homogeneously dispersed by analysis of corresponding energy dispersive X-ray spectroscopy (EDS) image, as shown in Fig. 11A. Furthermore, the rational proportions of hydrogen and ionic bonding could be optimized through changing the contents of HPC and Cu^{2+} to achieve maximum synergistic effect.

Compared with the pure GO and rGO film, the mechanical performances of rGO-HPC-Cu^{2+} reduced by HI solution was

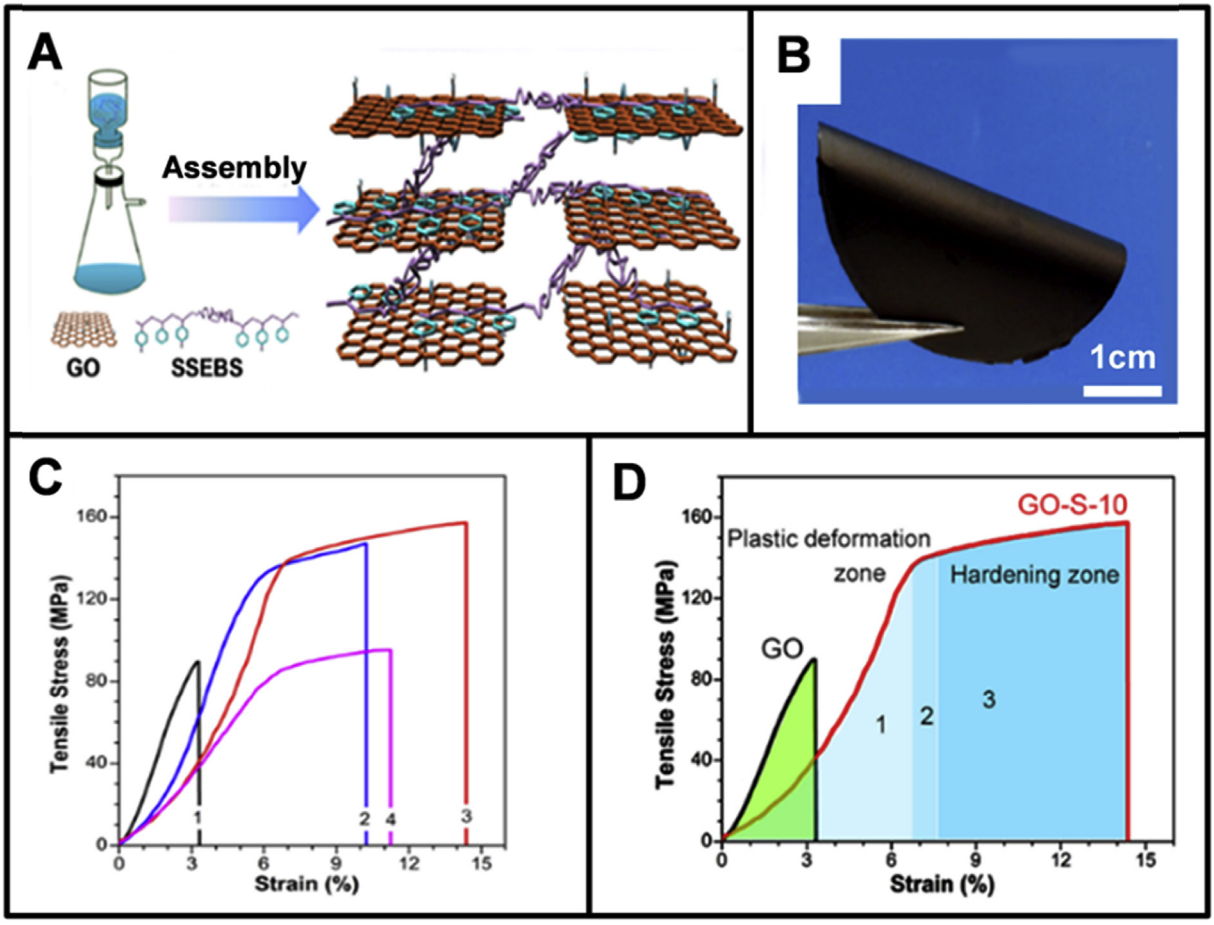

Fig. 10. Combination of hydrogen bonding and π-π interaction. (A) Schematic representation of the fabrication process of GO-SSEBS BPNs *via* vaccum-assisted filtration. (B) Digital photograph of GO-SSEBS-10. (C) Stress-strain curves of pure GO film (curve 1), GO-SSEBS-5 (curve 2), GO-SSEBS-10 (curve 3), and GO-SSEBS-15 (curve 4). (D) Typical stress-strain curves of pure SSEBS film and GO-S-10 polymer nanocomposites. Reproduced with permission [126].

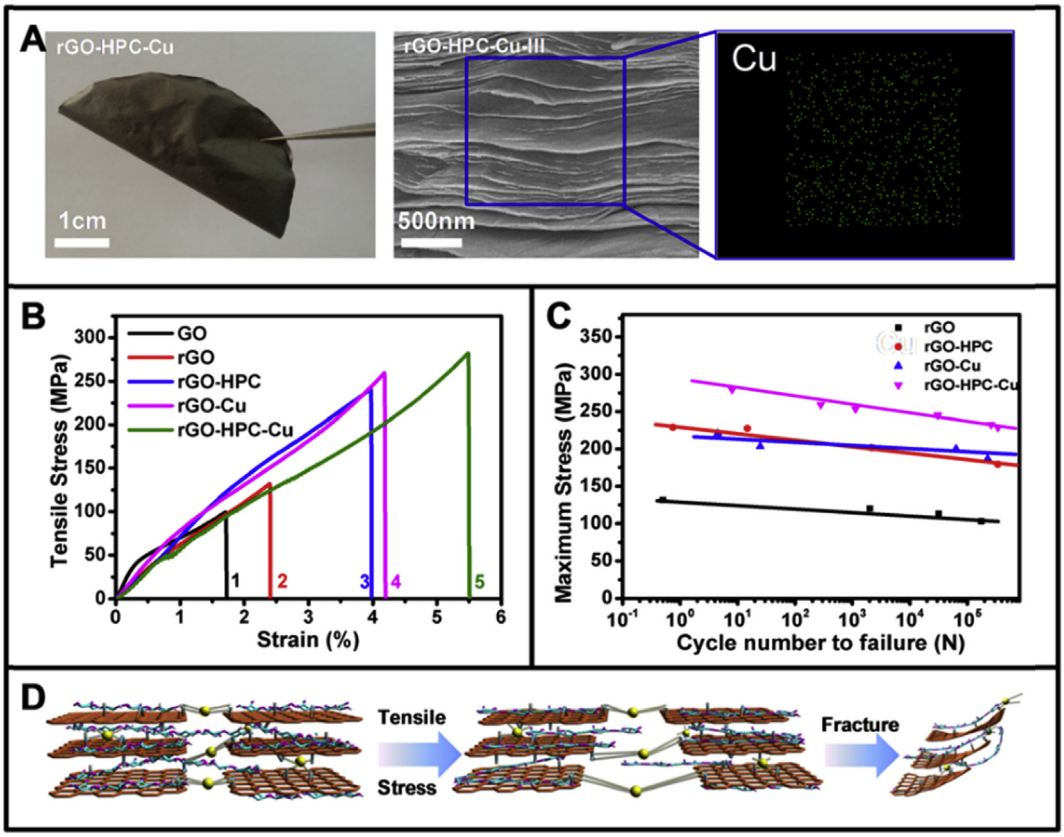

Fig. 11. Combination of hydrogen bonding and ionic bonding. (A) The digital photograph, the cross-section and Cu mapping of rGO-HPC-Cu bioinspired polymer nanocomposites. (B) The stress-strain curves of GO film (curve 1), rGO film (curve 2), rGO-HPC (curve 3), rGO-Cu (curve 4) and rGO-HPC-Cu (curve 5). (C) The maximum tensile stress versus the number of cycle-times to failure the pure rGO film, rGO-HPC, rGO-Cu and rGO-HPC-Cu. (D) The proposed fracture mechanism of rGO-HPC-Cu bioinspired polymer nanocomposites. Reproduced with permission [127].

dramatically improved, which were attributed to the synergistic effects from hydrogen and ionic bonding. The tensile strength and toughness of rGO-HPC-Cu^{2+} reached up to 274.3 MPa and 6.7 MJ m^{-3}, as shown in Fig. 11B. The synergistic effects of rGO-HPC-Cu^{2+} are evaluated by synergistic percentage (S) as follows [128]:

$$S = \frac{2\sigma_{hyb} - (\sigma_{HPC} + \sigma_{rGO})}{\sigma_{HPC} + \sigma_{rGO}} \times 100\%$$

where σ_{hyb}, σ_{HPC} and σ_{rGO} represent the tensile strength of rGO-HPC-Cu^{2+}, rGO-HPC and rGO films. The synergy percentage of rGO-HPC-Cu^{2+} reached maximum value of 331% and the fatigue properties of rGO-HPC-Cu^{2+} were much higher than rGO-HPC and rGO-Cu^{2+} at the same stress level by synergistic effects, as shown in Fig. 11C. The process of fracture could be divided into three stages: i) when loading, the hydrogen bonding of rGO-HPC-Cu^{2+} firstly ruptured and the coiled chains of HPC were stretched; ii) when further stretching, the ionic bonding of sample gradually fractured and parts of hydrogen bonding reformed. Moreover, humidity plays an important role during binding and rebinding of hydrogen as well as ionic crosslinks. Ionic crosslinks can also rebind at high humidity [116]; and iii) finally, the sample was totally destroyed. Therefore, the synergy from hydrogen and ionic bonding strategy could effectively fabricate excellent mechanical properties of BPNs, as shown in Fig. 11D. Moreover, because of the relatively low content of HPC (~3 wt %), the conductivity of BPNs was slightly lower than that of pure rGO film.

4.1.3. From hydrogen bonding and covalent bonding

The aforementioned strategies are synergy from non-covalent bonding. However, covalent bonding shows high strength and stability. In fact, the strong interfacial interactions can effectively transfer load, maintaining the integrity of structure. While, weak interfacial interactions can be constantly destroyed, causing the crack deflection, plastic deformation and other toughening mechanism. Therefore, synergy from non-covalent and covalent bonding is more suitable for constructing high integrated performance BPNs. For example, Cui et al. [88] successfully adopted DA, a mimic of mussel adhesive protein for constructing GO-PDA BPNs, as shown in Fig. 12A. The synergistic effect from covalent bonding and hydrogen bonding were formed between GO and PDA, and the tensile strength of rGO-PDA was improved to 204.9 MPa and the toughness reached up to 4.0 MJ m^{-3} with only about 4.6 wt % of PDA, which were much higher than that of nacre (80–135 MPa and 1.8 MJ m^{-3}), as shown in Fig. 12B. But, the electrical conductivity of rGO-PDA was 18.5 S cm^{-1}, which was much lower than that of pure rGO (44.8 S cm^{-1}).

Wan et al. demonstrated chitosan (CS) with many hydroxyl and amine functional groups could react with GO nanosheets to achieve high performance BPNs [129], as shown in Fig. 12C. The synergistic interfacial interactions were formed from hydrogen and covalent bonding with low CS content. Instead, "electrostatic stabilization" resulted in only hydrogen bonding with high CS content in GO-CS nanocomposites, as shown in Fig. 12D. The tensile strength of rGO-CS nanocomposites reached up to 526.7 MPa, which was higher than that of rGO-PDA nanocomposite with tensile strength of 204.9 MPa and was 4.9 times higher than GO and CS films, as

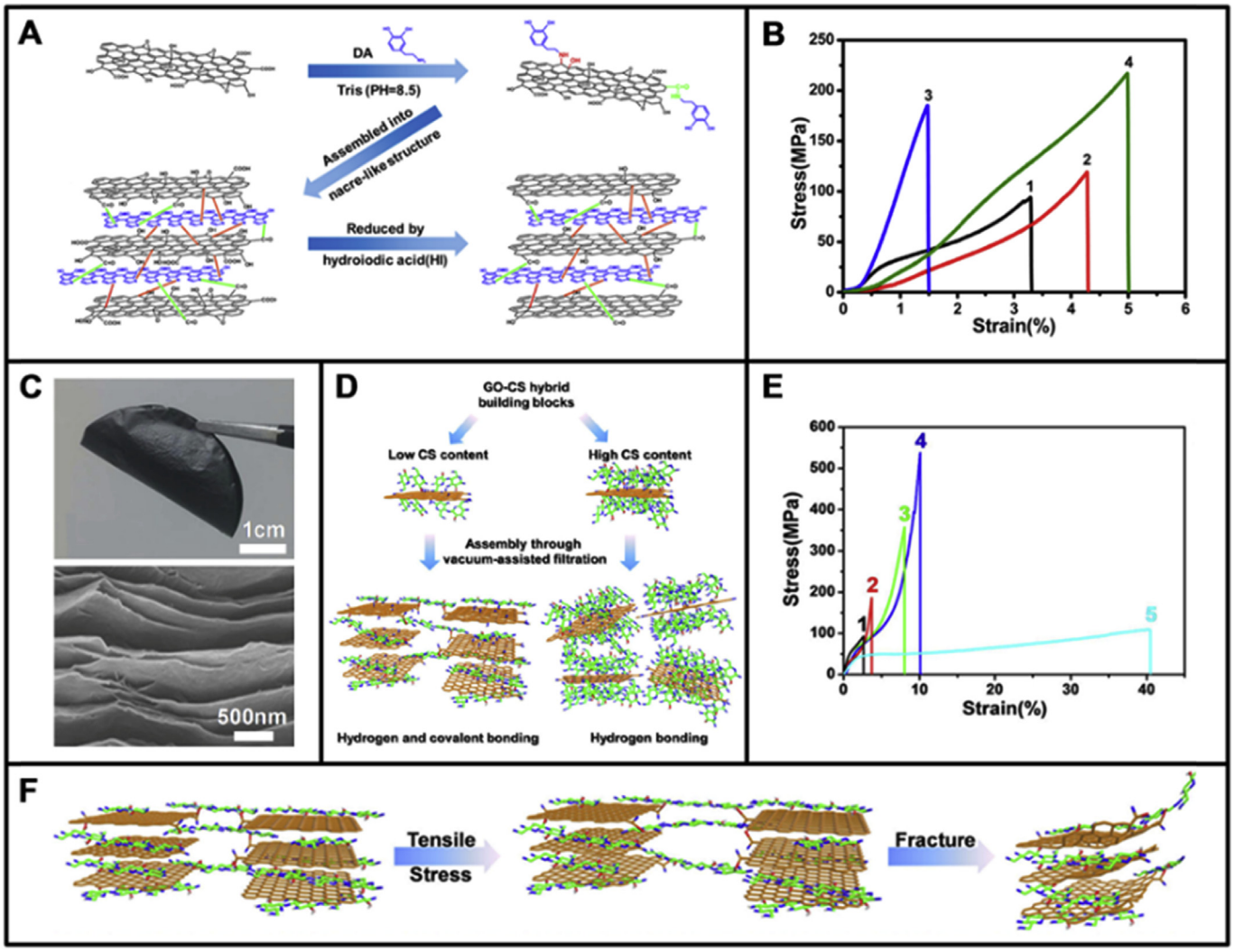

Fig. 12. Combination of hydrogen bonding and covalent bonding. (A) Illustration of the preparation process of the GO-PDA polymer nanocomposites. (B) Tensile stress curves of GO film (curve 1), rGO film (curve 2), GO-PDA-VI (curve 3), and GO-PDA-VI (curve 4). Reproduced with permission [88]. (C) A digital photograph and a cross-section SEM image of rGO-CS-V polymer nanocomposites. (D) Proposed mechanism of interfacial interactions between CS and GO nanosheets. (E) Stress-strain curves of GO films (curve 1), rGO film (curve 2), GO-CS-V (curve 3), rGO-CS-V (curve 4) and CS film (curve 5). (F) The proposed fracture mode of GO-CS-V polymer nanocomposites under loading. Reproduced with permission [129].

shown in Fig. 12E. In addition, the toughness of rGO-CS with 17.7 MJ m^{-3} was about 10 times higher than nacre. The high strength and toughness of rGO-CS nanocomposites were attributed to the synergy from hydrogen and covalent bonding. The proposed fracture process of rGO-CS nanocomposites is shown in Fig. 12F. With increased loading, the GO nanosheets slip, resulting in broken of hydrogen bonding, then the CS chains were stretched. Further stretching would lead to broken of the covalent bonding between CS and GO nanosheets, which resulted in the curling of edges of GO nanosheets. The excellent electrical conductivity of rGO-CS BPNs reached up to 155.3 S/cm. However, since the insulating CS molecules were embedded between rGO nanosheets, the electrical conductivity of BPNs was slightly lower than the pure rGO film.

The above results show that the tensile strength and toughness of rGO-CS nanocomposite [129] with synergy from hydrogen and covalent bonding are higher than that of rGO-HPC-Cu^{2+} nanocomposite [127] by synergy from hydrogen and ionic bonding. The synergy from ionic and covalent bonding was investigated in the next section.

4.1.4. From ionic bonding and covalent bonding

The mechanical performance of spider silk can be dramatically improved by introducing little of zinc ions [130]. Recently, Gong et al. [131] demonstrated great improvement in mechanical properties of GO-Zn^{2+}-PCDO BPNs. Zn^{2+} could form ionic bonding between GO nanosheets, and the covalent bonding was provided by PCDO molecules in rGO-Zn^{2+}-PCDO. Thus, the tensile strength and toughness were dramatically enhanced to 439.1 MPa and 7.5 MJ m^{-3}, as shown in Fig. 13A. In addition, the mechanical properties of rGO-Zn^{2+} with only ionic bonding and rGO-PCDO with only covalent bonding were lower than that of rGO-Zn^{2+}-PCDO. The main reason is the synergistic effect from ionic and covalent bonding. Meanwhile, the synergistic effect significantly improved the fatigue life of rGO-Zn^{2+}-PCDO, as shown in Fig. 13B. The energy dispersive spectroscopy (EDS) showed the element Zn was homogenous dispersion in the BPNs, as shown in Fig. 13C. The proposed fracture mechanism model of rGO-Zn^{2+}-PCDO BPNs was illustrated in Fig. 13D, which demonstrated the synergy from ionic and covalent bonding. When loading the sample, the ionic bonding

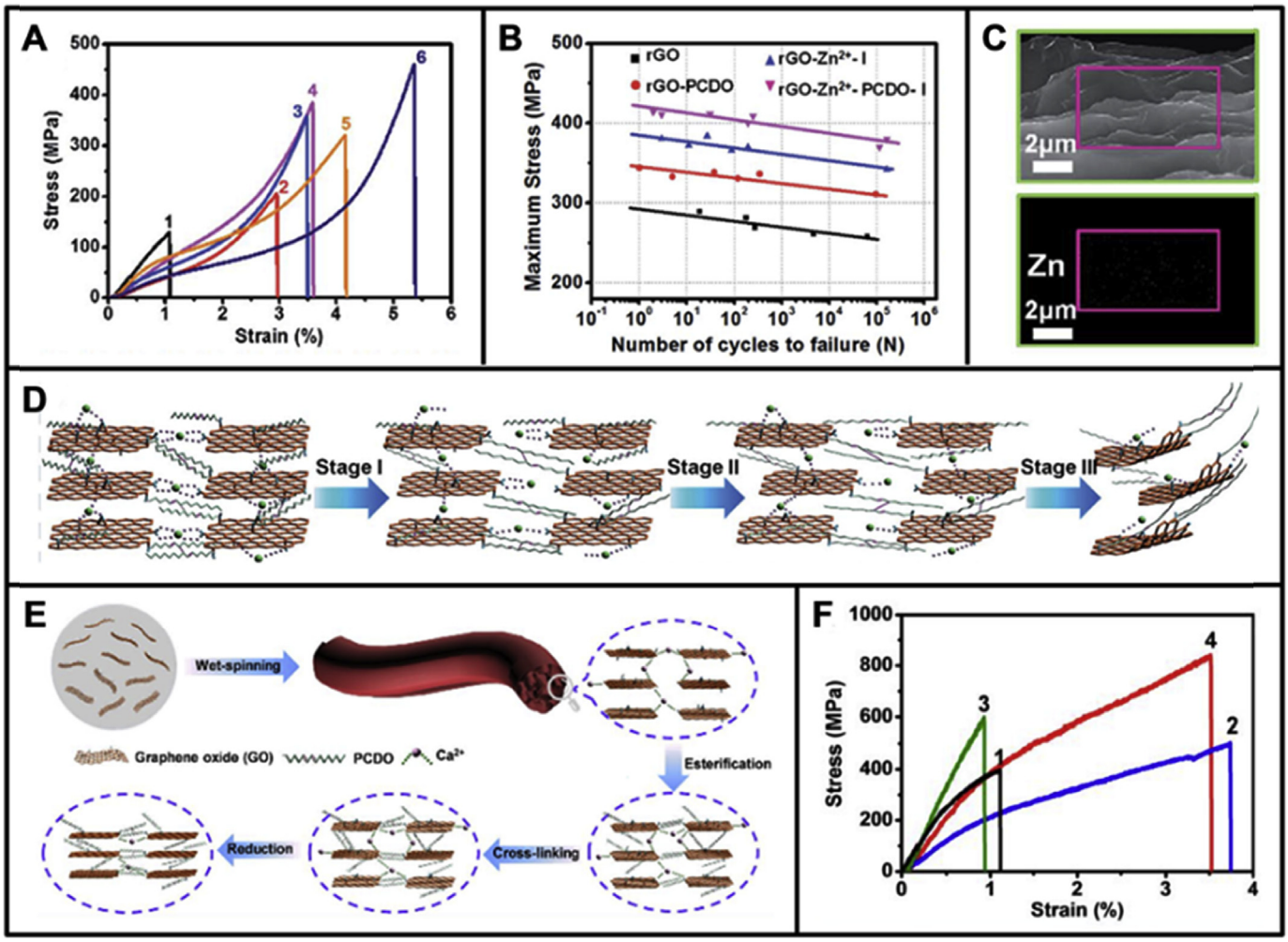

Fig. 13. Combination of ionic bonding and covalent bonding. (A) Strain-stress curves of GO film (curve 1), rGO film (curve 2), rGO-PCDO film (curve 3), rGO-Zn^{2+}-I film (curve 4), rGO-Zn^{2+}-I (curve 4), GO-Zn^{2+}-PCDO (curve 5) and rGO-Zn^{2+}-PCDO (curve 6). (B) Tensile fatigue testing of the rGO film, rGO-PCDO, rGO-Zn^{2+}-I, and rGO-Zn^{2+}-PCDO-I. (C) The fracture morphology of the rGO-Zn^{2+}-PCDO-I polymer nanocomposites. (D) The proposed fracture mechanism of the rGO-Zn^{2+}-PCDO polymer nanocomposites. Reproduced with permission [131]. (E) Schematic illustration of the preparation of the GO-Ca^{2+}-PCDO GBFs. (F) Stress-strain curves of GO-Ca^{2+}-II fiber (curve 1), rGO-Ca^{2+}-II fiber (curve 2), GO-Ca^{2+}-PCDO-II fiber (curve 3) and rGO-Ca^{2+}-PCDO-II fiber (curve 4). Reproduced with permission [132].

between Zn^{2+} and rGO nanosheets was firstly broken, and the long chains PCDO would extend along the slipping direction of rGO nanosheets. Further loading, the PCDO molecules were further stretched and the covalent and ionic bonding ruptured, dissipating much energy.

Wan et al. [132] demonstrated Chelate architecture in enhancing the fatigue life of BPNs through Ni^{2+} and polydopamine (PDA). The resultant of rGO-PDA-Ni^{2+} BPNs show the ultimate tensile strength of 417.2 MPa and toughness of 19.5 MJ m^{-3}, which were 2.1 and 7.5 folds of natural nacre, respectively. In addition, the electrical conductivity of rGO-PDA-Ni was kept very well as high as 144.5 S cm^{-1} after fatigue testing.

Synergistic effects from interfacial interactions are not only suitable for enhancing mechanical performance of BPNs, but also for graphene-based fibers (GBFs). Recently, Zhang et al. [133] constructed ultrastrong GBFs *via* synergistic effect from ionic and covalent bonding. In the wet spinning process, ionic bonding was formed between GO nanosheets by introducing Ca^{2+}, and PCDO was grafted on the surface of GO-Ca^{2+} fibers with annealing at different temperature. Then UV irradiation, the covalent bonding between PCDO molecules was formed, obtaining GO-Ca^{2+}-PCDO GBFs. After reduction by HI, the ultrastrong rGO-Ca^{2+}-PCDO GBFs were obtained, as shown in Fig. 13E. The resultant rGO-Ca^{2+}-PCDO GBFs showed the tensile strength as high as 842.6 MPa and the toughness of 15.8 MJ m^{-3}, as shown in Fig. 13F.

The aforementioned results reveal that the synergistic effects from interfacial interactions could dramatically improve the mechanical properties and electrical conductivity of BPNs. Nevertheless, precisely tuning the synergy from interfacial interactions of BPNs remains a great challenge. Except for the synergistic effects from interfacial interactions, synergy from building blocks are also important for enhancing the performance of BPNs.

4.2. Synergistic effects from building blocks

1D nanofibrillar chitin and 2D aragonite calcium platelets play a key role in the mechanical properties of nacre [28]. Inspired by the unique structure of nacre, ternary BPNs were constructed and the synergistic effects from building blocks were also demonstrated for improving mechanical performance. In our group, 1D building blocks DWNTs and nanofibrillar cellulose (NFC) are used to prepare GO based and MMT based BPNs. 2D molybdenum disulfide (MoS_2) and MMT are utilized for fabricating GO based BPNs by synergy from building blocks. In the following sections, these ternary BPNs

were discussed in detail.

4.2.1. From 1D building blocks

Gong et al. [95] prepared integrated ternary rGO-DWNTs-PCDO BPNs, as shown in Fig. 14A. DWNTs played a critical role in improving the tensile strength and toughness of resultant BPNs. The tensile strength and toughness of rGO-DWNTs-PCDO were 235.3 MPa, and 6.9 MJ m^{-3}, respectively, as shown in Fig. 14B. The fatigue life of rGO-DWNTs-PCDO was almost 5 orders of magnitude than GO-DWNTs at the same stress level, as shown in Fig. 14C. The main reason should be attributed to the synergistic effects from building blocks and covalent bonding. The crack propagation were synergistically restrained by deflection of rGO nanosheets and bridging of DWNTs. This kind of synergistic crack suppression mechanisms could increase the energy dissipation and improve fatigue life.

On the other hand, Gong et al. [96] also designed rGO-DWNTs-PVA ternary BPNs through constructing synergistic effect from building blocks and hydrogen bonding. The tensile strength reached 323.0 MPa and the toughness was 11.3 MJ m^{-3} as shown in Fig. 14D. The rGO-DWNTs-PVA also showed excellent fatigue resistance performance as shown in Fig. 14E. The possible fracture mechanism was proposed in Fig. 14F. When stretching, rGO nanosheets started to slip, and then, DWNTs and PVA bridged the crack and prevented the further sliding of rGO nanosheets. Further loading, the hydrogen bonding was broken and DWNTs were pulled out, resulting in fracture and much more energy dissipation.

NFC derived from wood shows high elastic modulus of ~150 GPa with abundant hydroxyl groups, which is chosen as 1D building blocks for constructing ternary BPNs with GO and PCDO. Duan et al. [134] fabricated rGO-NFC-PCDO ternary BPNs with synergistic effects from building blocks, hydrogen and covalent bonding, as shown in Fig. 15A. The tensile strength and toughness of rGO-NFC-PCDO were 314.6 MPa, and 9.8 MJ m^{-3}, respectively, as shown in Fig. 15B. The rGO-NFC-PCDO with high electrical conductivity, can be utilized as conductive wire in a circuit, as shown in Fig. 15C. The proposed fracture mechanism was shown in Fig. 15D. When stretching, the hydrogen bonding was firstly broken between rGO and NFC. The NFC was pulled out after further loading, dissipating much more energy. Finally, covalent bonding of PCDO and rGO nanosheets was broken.

On the other hand, the synergistic effect also be demonstrated in other ternary BPNs, for example, Wang et al. [33] demonstrated transparent ternary MMT-NFC-PVA film as shown in Fig. 16A. The hierarchical structure is proposed as Fig. 16B. This kind of ternary MMT-NFC-PVA film showed excellent mechanical properties compared with other binary BPNs. The tensile strength, Young's modulus and toughness of MMT-NFC-PVA reach 302 MPa, 22.8 GPa and 3.72 MJ m^{-3}, respectively, as shown in Fig. 16C. The fatigue life of ternary MMT-NFC-PVA was 2 and 4 orders of magnitude higher than that of binary NFC-PVA and MMT-PVA at the same stress level, as shown in Fig. 16D. A crack mechanism of MMT-NFC-PVA was illustrated in Fig. 16E. i) MMT nanoplatelets resisted the crack propagation by deflection and ii) the NFC fibril bridged the crack to suppress crack propagation; iii) when further loading, the MMT nanoplatelets and NFC were pulled out and the sample fractured.

4.2.2. From 2D building blocks

The 2D MoS_2 nanosheets have outstanding catalytic, lubricant and mechanical physical properties [135]. Wan et al. [94] constructed integrated strength and toughness ternary rGO-MoS_2-thermoplastic urethane (TPU). The ternary layered structure of rGO-MoS_2-TPU was prepared by vacuum assisted-filtration, as shown in Fig. 17A. When the content of MoS_2 was about 4 wt %, the maximum mechanical properties of rGO-MoS_2-TPU were achieved. The tensile strength and toughness of rGO-MoS_2-TPU were 235.3 MPa, and 6.9 MJ m^{-3}, respectively, as shown in Fig. 17B, which were 40% and 100% higher than rGO—TPU binary composites and 1.7 and 3.8 of natural nacre. The proposed crack propagation model is illustrated in Fig. 17C. The hydrogen bonding between rGO nanosheets and TPU was firstly broken when stretching. Then, crack propagation would be deflected by MoS_2 nanosheets, due to

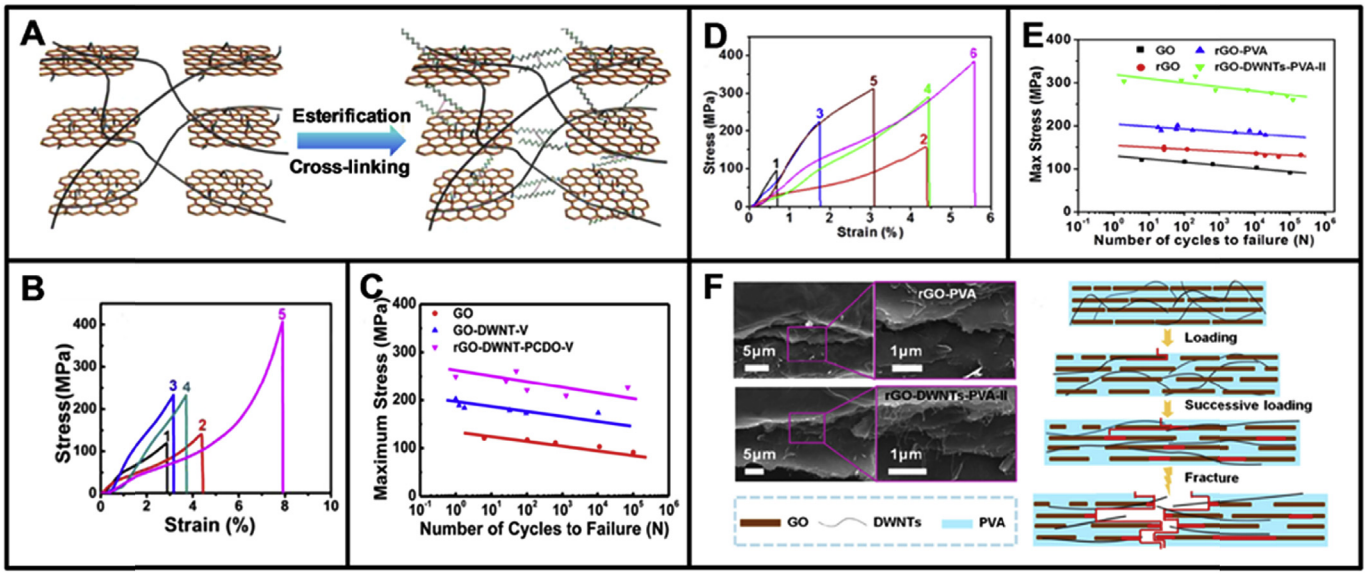

Fig. 14. (A) Schematic illustration of process for preparing GO-DWNT-PCDO polymer nanocomposites. (B) Typical strain-stress curves of GO film (curves 1), rGO films (curves 2), GO-DWNT-V (curves 3), GO-DWNT-PCDO-V (curves 4) and rGO-DWNT-PCDO-V (curves 5). (C) Tensile fatigue testing of GO film, GO-DWNT and rGO-DWNT-PCDO-V. Reproduced with permission [95]. (D) Tensile stress-strain curves of pure GO film (curves 1), rGO film (curves 2), GO-PVA (curves 3), rGO-PVA (curves 4), GO-DWNT-PVA-II (curves 5) and rGO-DWNT-PVA-II (curves 6). (E) S-N curves in pure tension pattern for pure GO film, rGO-PVA and rGO-DWNT-PVA-II. (F) The fracture morphologies of rGO-PVA and rGO-DWNTs-PVA-II and the fracture mechanism for rGO-DWNTs-PVA-II polymer nanocomposites. Reproduced with permission [96].

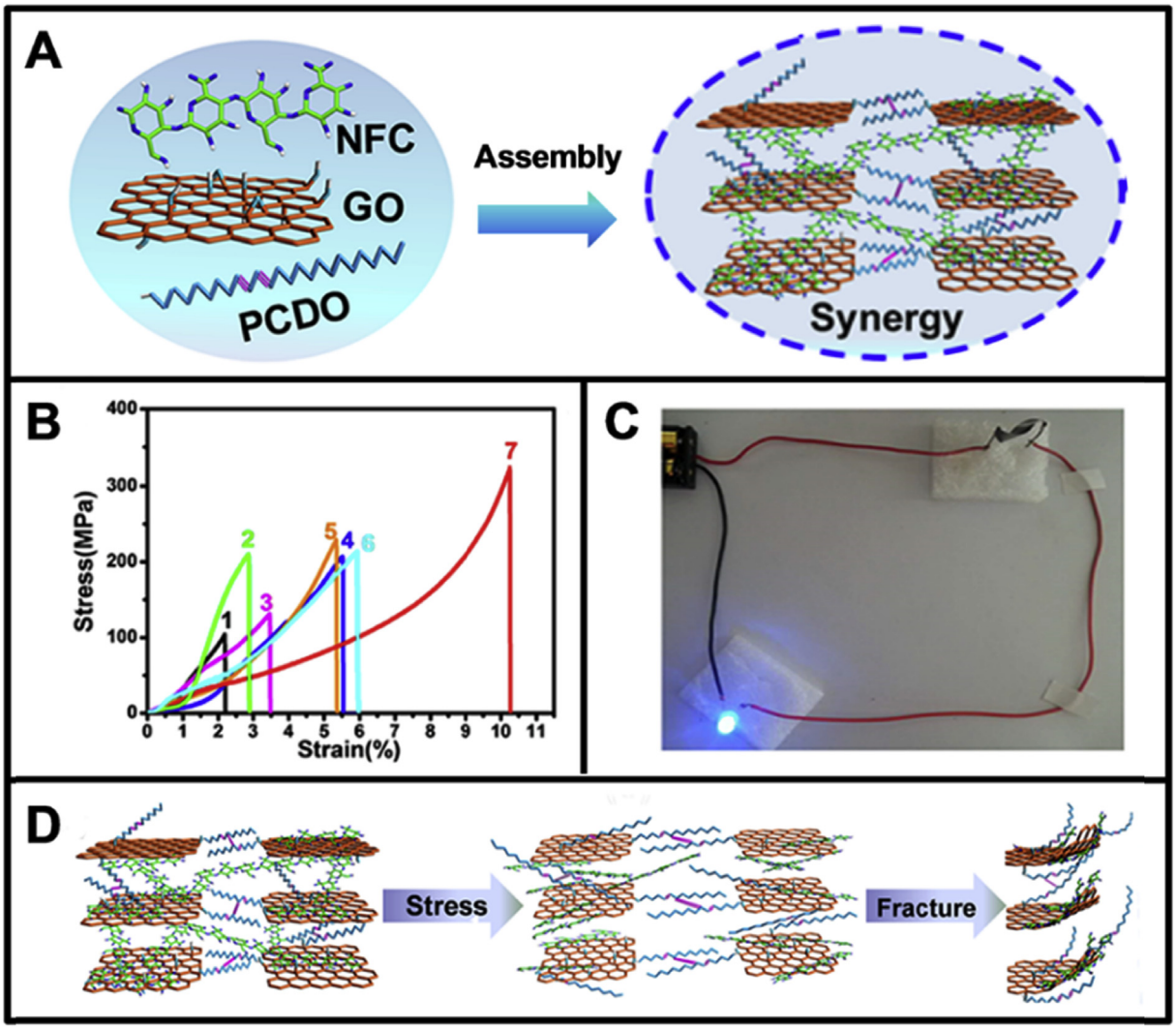

Fig. 15. (A) Schematic illustration of process for preparing GO-NFC-PCDO polymer nanocomposites. (B) Typical stress-strain curves of GO film (curve 1), NFC film (curve 2), rGO film (curve 3), GO-NFC-IV (curve 4), GO-NFC-PCDO-IV (curve 5), rGO-NFC-IV (curve 6) and rGO-NFC-PCDO-IV (curve 7). (C) The digital photo of circuit. (D) The proposed fracture mechanism of rGO-NFC-PCDO-IV. Reproduced with permission [134].

the lubrication of 2H MoS_2, absorbing much energy. When further loading, the crack propagation was continually deflected until the rGO-MoS_2-TPU fractured. The optimized content of MoS_2 is about 4.0 wt%. When below than 4.0 wt%, MoS_2 could not effectively deflect crack, leading to less improvement in mechanical properties. When higher than 4.0 wt %, excessive stacking of MoS_2 resulted in low efficiency of stress transfer and energy dissipation.

In addition to the excellent mechanical properties, synergy from building blocks could also provide other properties such as fire retardant. For example, Ming et al. [136] have demonstrated fire retardant rGO-MMT-PVA ternary BPNs by vacuum-assisted filtration. MMT was well dispersion in rGO-MMT-PVA, which is confirmed by EDS of Si element, as shown in Fig. 18A. The tensile strength and toughness reached up to 356.0 MPa, and 7.5 MJ m^{-3}, as shown in Fig. 18B. Meanwhile, the excellent fatigue resistant properties comparable to binary rGO-MMT is shown in Fig. 18C. The rGO-MMT-PVA could protect silk cocoon from burning, as shown in Fig. 18D and E. The rGO-MMT-PVA burnt and generated gas due to the PVA and residual oxygen groups of rGO when the film was exposed to the flame. After that, the film form inorganic interlocked framework and did not burn any more.

5. Representative applications

BPNs with integrated mechanical and electrical properties show great potential of application in many fields, such as filter [137], sensors [138], energy storage [139], actuators [140], organic photovoltaic devices [141] and electromagnetic interference (EMI) shielding [142] etc. For example, Hu et al. [137] reported a new water separation film that water could flow through and unwanted solutes were rejected. The film was made of GO nanosheets *via* layer-by-layer deposition and then cross-linked through 1, 3, 5-benzenetricarbonyl trichloride. The GO film was supported on the polydopamine coated polysulfone and showed a high rejection of Rhodamine-WT. The results of flux were 4–10 times higher than that of most commercial nanofiltration films, as shown in Fig. 19A. Guo et al. [143] prepared MMT-hydroxyethyl cellulose (HEC) BPNs by mimicking columnar nacre. The BPNs with columnar structure on its surface showed high mechanical performance and underwater low oil adhesion, which can be used as underwater oil-repellent materials.

BPNs based electrochemical sensors and biosensors [144,145] are illustrated in Fig. 19B. Huang et al. [138] indicated graphene

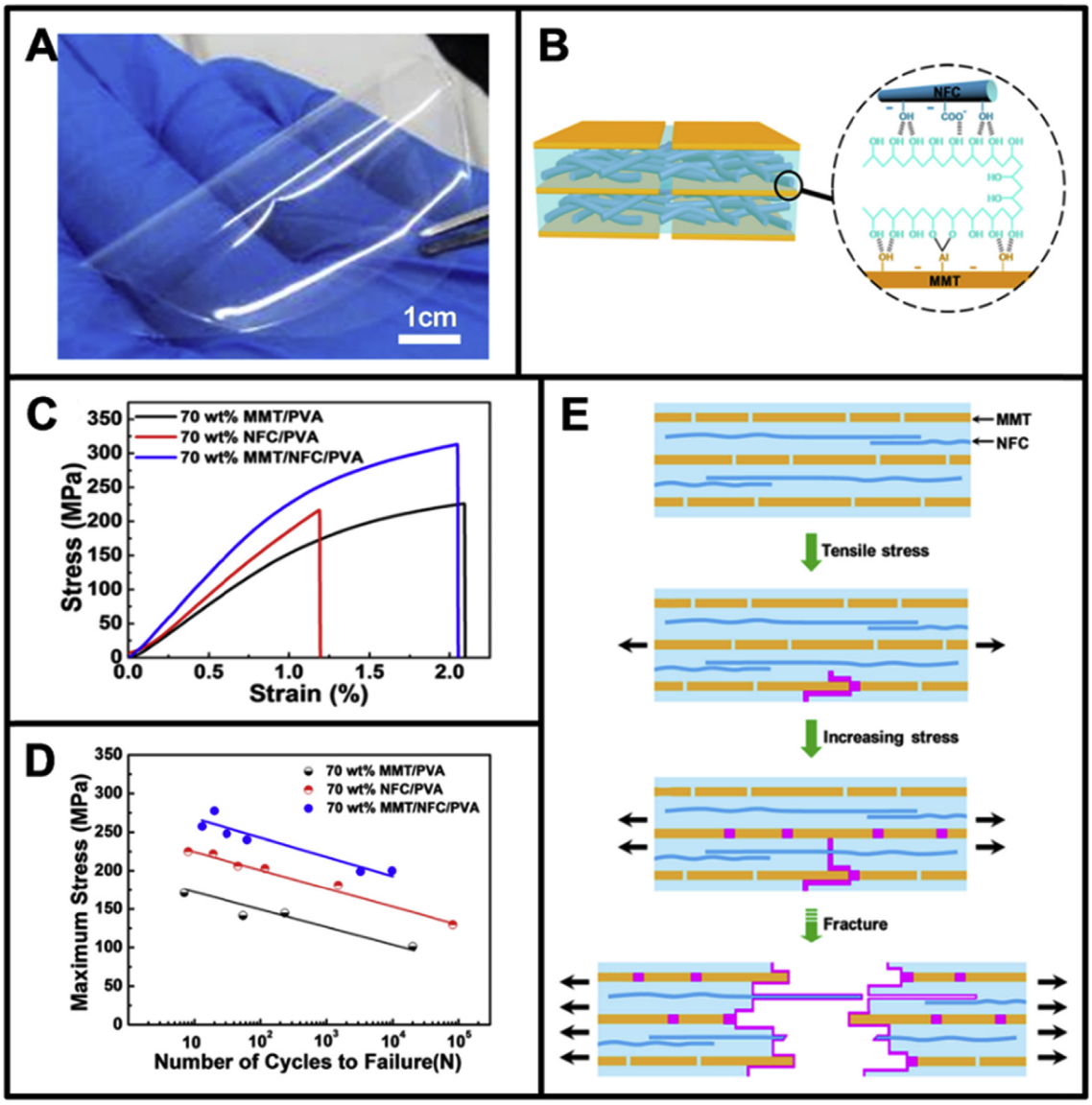

Fig. 16. (A) Digital photo of MMT-NFC-PVA polymer nanocomposites. (B) Propsosed structural model of MMT-NFC-PVA. (C) Stress-strain curves of MMT-PVA (black curve), NFC-PVA (red curve) and MMT-NFC-PVA (blue curve). (D) Maximum stress vs number of cycles to failure in pure tension mode for MMT-PVA, NFC-PVA and MMT-NFC-PVA (blue curve). (E) Proposed synergistic mechanism of 2D MMT platelets and 1D NFC fibrils. Reproduced with permission [33]. (For interpretation of the references to colour in this figure legend, the reader is referred to the web version of this article.)

as a candidate for nanoelectronic biosensors to detect the glucose or glutamate molecules. Large-sized CVD grown graphene films were prepared as field-effect transistors and specific redox enzymes were functionalized onto the graphene films. Because glucose or glutamate molecules could produce H_2O_2 by the catalytic reactions of enzymes, which can increase the conductivity of graphene, they could be detected the change of conductance of graphene transistor. Besides detecting the glucose or glutamate, graphene also are utilized for dopamine (DA) sensor. For instance, Xie et al. [146] prepared rGO-Polyaniline (PANI)-nafion (NF) nanocomposites to detect DA by applying differential pulse voltammetry. The rGO-PANI-NF with good catalytic activity showed excellent selectivity toward DA even if there were ascorbic acid and uric acid.

Good mechanical flexibility, high conductivity and excellent cycle capability of energy storage devices are urgently needed in electronic devices. Owing to the stability and high conductivity of grahene under ambient conditions, it is the ideal candidate for constructing energy storage materials. Lu et al. [139] demonstrated flexible graphene-polypyrrole (PPy)-CNTs ternary BPNs as supercapacitors, as shown in Fig. 19C. The flexible GN and rigid CNTs could significantly improve the electronic conductivity and excellent cycling stability of the nanocomposites. The *Cm* and Cv of GN-PPy-CNTs were 211Fg^{-1} and 122 Fcm^{-3}, respectively, which were much higher than those of GN and PPy-CNTs.

BPNs as actuator systems are urgently needed for applications such as robots, sensors and memory chips. For instance, one side of the graphene film was treated with hexane plasma [140], enhancing the surface hydrophobicity, and the other side was exposed to O_2 plasma, becoming hydrophilic, as shown in Fig. 19D. Because of the asymmetric surface performance of graphene film, it would induce the distinction of electrochemical response and produce the driving force of the actuation behavior [142].

Organic photovoltaic (OPV) devices as the solar energy

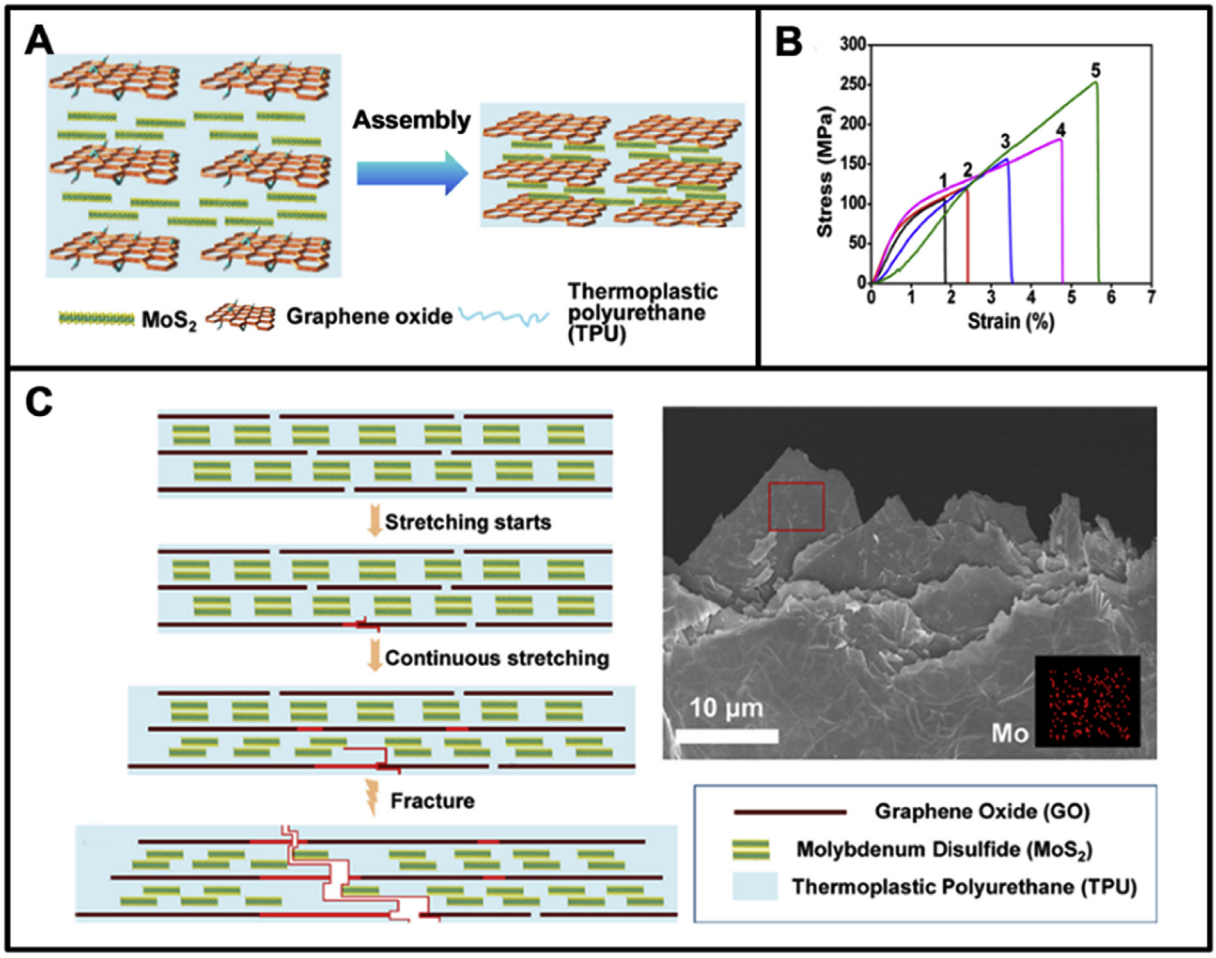

Fig. 17. Illustration of preparation process of GO-MoS_2-TPU polymer nanocomposites. (B) Tensile stress-strain curves of GO film (curve 1), GO-TPU (90:10) (curve 2), rGO-TPU (curve 3), GO-MoS2-TPU-II (curve 4) and rGO-MoS2-TPU-II (curve 5). (C) Proposed synergistic mechanism and fracture morphology of rGO-MoS2-TPU. Reproduced with permission [94].

harvesting platforms have many unique characteristics, as shown in Fig. 19E, which attract widely attentions of researchers. For example, Yin et al. [133] prepared flexible and laminated structure of graphene films (rGO-PET), which was used as a transparent electrode of OPV devices. The preparation of rGO-PET was reduction GO film and transferred onto the PET. When the optical transmittance of rGO >65%, OPV device property depended on the resistance of rGO film, i.e. the charge transport efficiency. While, if the optical transmittance of rGO was lower than 65%, the light transmission efficiency determined the device performance. The rGO-PET could sustain a thousand cycles of bending owing to the flexibility of rGO.

BPNs could also work as electromagnetic interference (EMI) shielding to meet working requirements of electronic communication devices, such as computers, phones etc. as shown in Fig. 19F. For instance, Song et al. [142] fabricated multilayer graphene (MLG)-ethylene-vinyl acetate copolymers (EVA) film with mechanical flexibility and investigated the mechanism of adsorption and reflection. In order to evaluate EMI shielding, the MLG-EVA film was casted onto the paraffin-PVA substrates, forming sandwich structures. The results suggested that reflection dominated shielding mechanism and the thickness, skin depth and electrical conductivity of MLG-EVA were also important factors to improve the EMI shielding. The optimized shielding effectiveness of MLG-EVA is 27 dB that could effectively shield the interference.

6. Summary and outlook

MMT with high mechanical properties and fire resistant is used to prepare MMT-based polymer nanocomposites that have potential applications in the automotive, aerospace. Because of CNTs' excellent mechanical, electrical and thermal properties, CNTs-based polymer nanocomposites can be applied in stealth, electromagnetic shielding and absorbing materials. GO-based polymer nanocomposites show high mechanical, electrical and thermal properties after reduction, attributing to the unique physicochemical performance of graphene nanosheets. In the field of supercapacitors and flexible electrode materials, GO-based polymer nanocomposites are one of the best candidates.

The feature article summaries the methods and surface modification of traditional polymer nanocomposites (TPNs) briefly and points out the issues of poor dispersion, random structure, low nonofillers content and weak interfacial interactions between polymer and nonofillers in TPNs. To efficiently solve the problem, bioinspried strategy has been proposed inspiring by the hierarchical structure of nacre. We fabricated FDWCNT-based, MMT-based and GO-based bioinspired polymer nanocomposites *via* different assembly approaches. Compared with traditional methods, the advantages of bioinspired assembly approaches for constructing polymer nanocomposites are as follows: i) well-dispersion of building blocks and polymer; ii) well-ordered

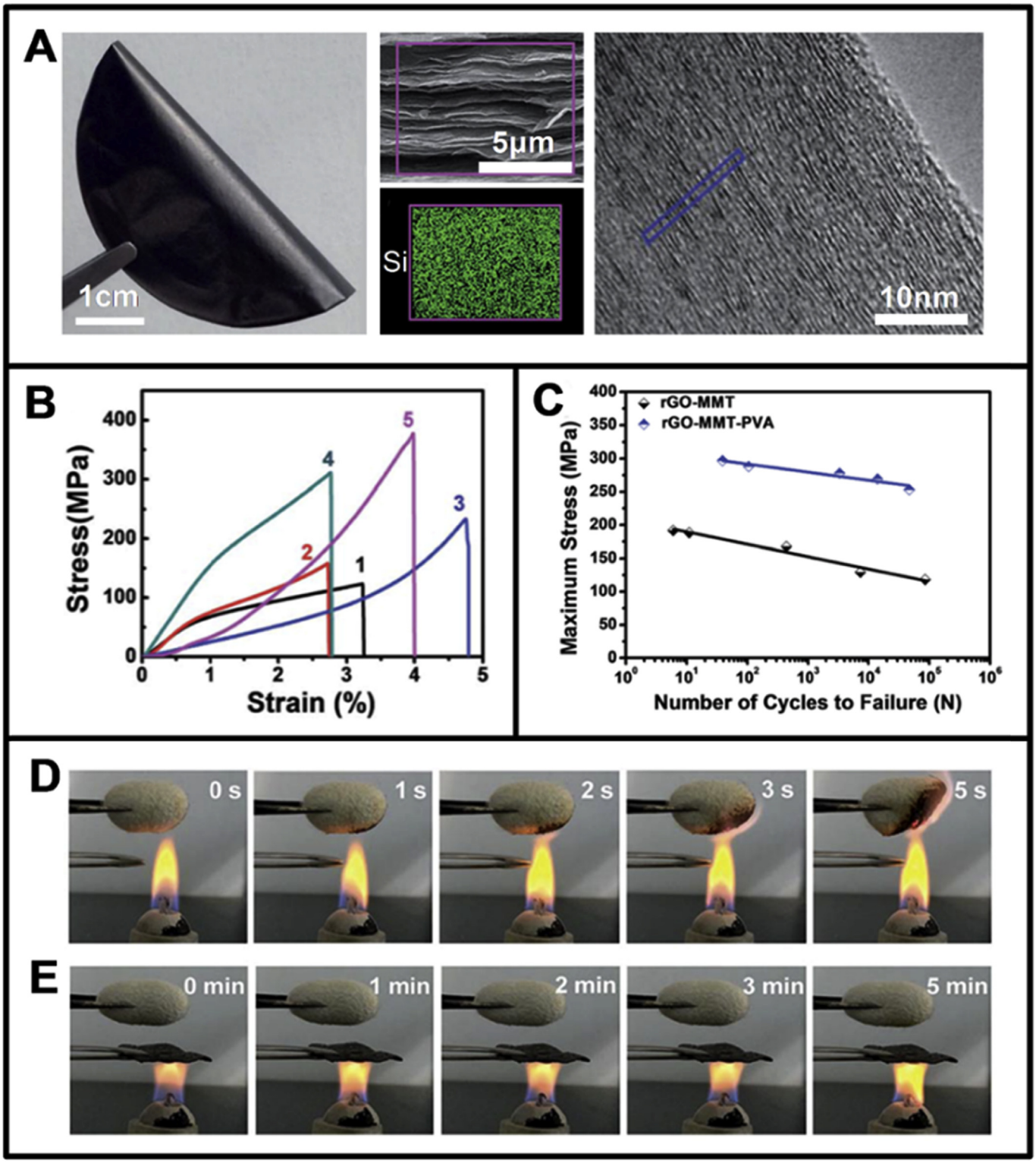

Fig. 18. (A) Digital image, SEM image of the cross-section, Si mapping and the high resolution TEM image of the cross-section of GO-MMT-PVA polymer nanocomposites. (B) Tensile stress-strain curves of the GO film (curve 1), GO-MMT-VI (90:10) (curve 2), rGO-MMT-VI (curve 3), GO-MMT-PVA-IV (curve 4) and rGO-MMT-PVA-IV (curve 5). (C) Maximum stress-number of cycles to failure in tension mode for the rGO-MMT and rGO-MMT-PVA. (D) (E) Ternary rGO-MMT-PVA polymer nanocomposites act as a fire shield to protect a silk cocoon. Reproduced with permission [136].

hierarchical structure; iii) high content of building blocks; and iv) designable interfacial interactions and building blocks. Meanwhile, we discussed interfacial interactions including non-covalent bonding (hydrogen bonding, ionic bonding and π-π interaction) and covalent bonding (linear molecule and polymer, branched polymer and 3D network) in details. The works of our group mainly design the synergy from interfacial interactions and building blocks for further improvement of the mechanical properties. These

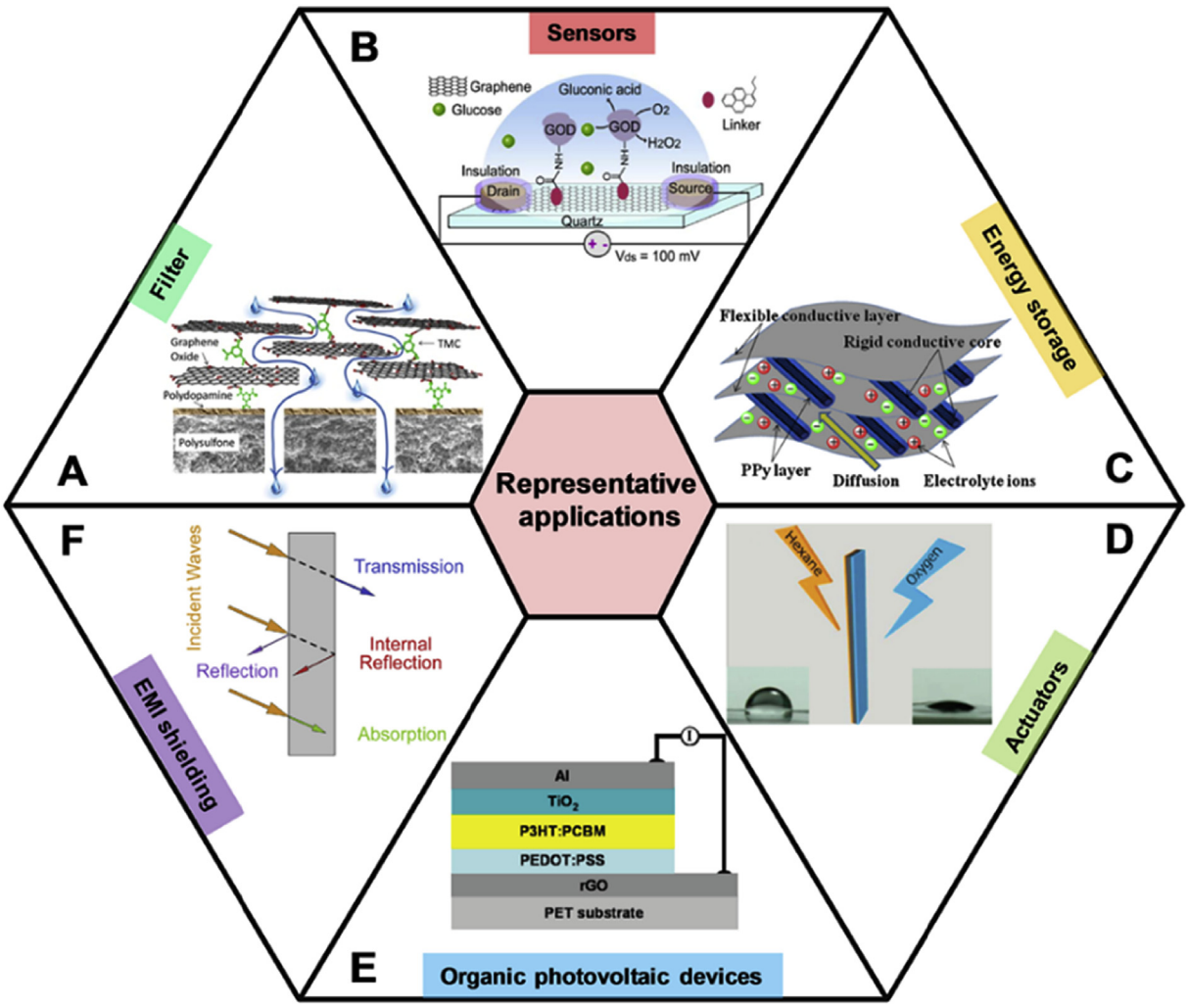

Fig. 19. BPNs could be utilized in many fields such as (A) Filter for separating water and unwanted solutes. Reproduced with permission [137]. (B) Sensors for detecting glucose or glutamate molecules. Reproduced with permission [145]. (C) Energy storages are urgently needed in electronic devices. Reproduced with permission [139]. (D) BPNs as actuators produce a driving force. Reproduced with permission [140]. (E) Organic photovoltaic devices for harvesting solar energy. Reproduced with permission [141]. (F) Electromagnetic interference (EMI) shielding for shielding the interference. Reproduced with permission [142].

synergistic effects also produce additional performances such as high fatigue and fire resistant properties, which means bioinspired strategy for polymer nanocomposites is viable and practical. Finally, the representative applications of bioinspired polymer nanocomposites (BPNs) are introduced simply in this paper, such as filter, sensors, energy storage and actuators.

At present, the BPNs cannot achieve the perfect performances like natural materials, and various synthetic effects and multiscale mechanisms in biological materials cannot be exactly reproduced by BPNs. However, the ultimate goal of BPNs is not a simple mimicking the structure of natural materials. The key is to introduce the strength and toughness mechanism of natural materials into the BPNs, and employ the principle to fabricate lightweight, high strength and super tough BPNs. In other words, our goal is to prepare the high mechanical properties and functional even intelligent materials by adjusting the structure and interfacial interactions. In the near future, the BPNs maybe to realize applications in aerospace as structural materials, in wearable electric devices as functional materials and in intelligent devices. Meanwhile, novel hybrid structures of BPNs with urgently needed properties would be achieved and simple, low-cost and effective method could be developed to fabricate high performances, multifunctional and larger-scale BPNs. Although there are many challenges and issues of fabricating BPNs, it could be anticipated that BPNs are the development direction of polymer nanocomposites.

Acknowledgements

This work was supported by the Excellent Young Scientist Foundation of NSFC (51522301), the National Natural Science Foundation of China (21273017, 51103004), the Program for New Century Excellent Talents in University (NCET-12-0034), the Fok Ying Tong Education Foundation (141045), the Open Project of Beijing National Laboratory for Molecular Sciences, the 111 Project (B14009), the Aeronautical Science Foundation of China (20145251035, 2015ZF21009), State Key Laboratory of Organic-Inorganic Composites (oic-201701007), Beijing University of Chemical Technology (oic-201701007), the State Key Laboratory for Modification of Chemical Fibers and Polymer Materials, Donghua University (LK1508), and the Fundamental Research Funds for the Central Universities (YWF-16-BJ-J-09, YWF-17-BJ-J-33).

References

[1] S. Komarneni, Nanocomposites, J. Mater. Chem. 2 (12) (1992) 1219–1230.
[2] G.M. Whitesides, Nanoscience, nanotechnology, and chemistry, Small 2 (1) (2005) 172–179.
[3] R.N. Kostoff, R.G. Koytcheff, C.G.Y. Lau, Global nanotechnology research literature overview, Technol. Forecast. Soc. 74 (9) (2007) 1733–1747.
[4] M.C. Roco, W.S. Bainbridge, Societal implications of nanoscience and nanotechnology: maximizing human benefit, J. Nanopart. Res. 7 (1) (2005) 1–13.
[5] J. Jordan, K.I. Jacob, R. Tannenbaum, M.A. Sharaf, I. Jasiuk, Experimental trends in polymer nanocomposites—a review, Mater. Sci. Eng. A 393 (1–2) (2005) 1–11.
[6] S. Pavlidou, C.D. Papaspyrides, A review on polymer–layered silicate nanocomposites, Prog. Polym. Sci. 33 (12) (2008) 1119–1198.
[7] G. Mittal, V. Dhand, K.Y. Rhee, S.-J. Park, W.R. Lee, A review on carbon nanotubes and graphene as fillers in reinforced polymer nanocomposites, J. Ind. Eng. Chem. 21 (2015) 11–25.
[8] P.C. Ma, N.A. Siddiqui, G. Marom, J.K. Kim, Dispersion and functionalization of carbon nanotubes for polymer-based nanocomposites: a review, Compos. Part A Appl. S 41 (10) (2010) 1345–1367.
[9] K. Hu, D.D. Kulkarni, I. Choi, V.V. Tsukruk, Graphene-polymer nanocomposites for structural and functional applications, Prog. Polym. Sci. 39 (11) (2014) 1934–1972.
[10] G. Mittal, V. Dhand, K.Y. Rhee, S.J. Park, W.R. Lee, A review on carbon nanotubes and graphene as fillers in reinforced polymer nanocomposites, J. Ind. Eng. Chem. 21 (1) (2014) 11–25.
[11] J.H. Lee, J. Marroquin, K.Y. Rhee, S.J. Park, D. Hui, Cryomilling application of graphene to improve material properties of graphene/chitosan nanocomposites, Compos. Part B-Eng 45 (1) (2013) 682–687.
[12] A. Liu, A. Walther, O. Ikkala, L. Belova, L.A. Berglund, Clay nanopaper with tough cellulose nanofiber matrix for fire retardancy and gas barrier functions, Biomacromolecules 12 (2011) 633–641.
[13] J.J. Kochumalayil, M.B. Wohlert, S. Utsel, L. Wågberg, Q. Zhou, L.A. Berglund, Bioinspired and highly oriented clay nanocomposites with a xyloglucan biopolymer matrix: extending the range of mechanical and barrier properties, Biomacromolecules 14 (2013) 84–91.
[14] Z. Spitalsky, D. Tasis, K. Papagelis, C. Galiotis, Carbon nanotube–polymer composites: chemistry, processing, mechanical and electrical properties, Prog. Polym. Sci. 35 (3) (2010) 357–401.
[15] J.H. Chang, D.K. Park, K.J. Ihn, Montmorillonite-based nanocomposites of polybenzoxazole: synthesis and characterization (I), J. Polym. Sci. Part B Poly. Phys. 39 (5) (2001) 471–476.
[16] B. Chen, J. Evans, Poly(epsilon-caprolactone)-clay nanocomposites: structure and mechanical properties, Macromolecules 39 (2) (2006) 747–754.
[17] I.S. Helical, Microtubeles of graphic carbon, nature 354 (6348) (1991) 56–58.
[18] L. Liu, A.H. Barber, S. Nuriel, H.D. Wagner, Mechanical properties of functionalized single-walled carbon-nanotube/poly(vinyl alcohol) nanocomposites, Adv. Funct. Mater 15 (6) (2005) 975–980.
[19] D. Wang, P. Song, C. Liu, W. Wu, S. Fan, Highly oriented carbon nanotube papers made of aligned carbon nanotubes, Nanotechnology 19 (7) (2008) 075609.
[20] K. Jiang, Q. Li, S. Fan, Nanotechnology: spinning continuous carbon nanotube yarns, Nature 419 (6909) (2002) 801.
[21] J. Zou, X. Zhang, J. Zhao, C. Lei, Y. Zhao, Y. Zhu, Q. Li, Strengthening and toughening effects by strapping carbon nanotube cross-links with polymer molecules, Comp. Sci. Tech. 135 (2016) 123–127.
[22] L. Zhang, X. Wang, R. Li, Q. Li, P.D. Bradford, Y. Zhu, Microcombing enables high-performance carbon nanotube composites, Comp. Sci. Tech. 123 (2015) 92–98.
[23] Y. Zhang, S. Gong, Q. Zhang, P. Ming, S. Wan, J. Peng, L. Jiang, Q. Cheng, Graphene-based artificial nacre nanocomposites, Chem. Soc. Rev. 45 (9) (2016) 2378–2395.
[24] S. Stankovich, D.A. Dikin, G.H.B. Dommett, K.M. Kohlhaas, E.J. Zimney, E.A. Stach, R.D. Piner, S.T. Nguyen, R.S. Ruoff, Graphene-based composite materials, Nature 442 (7100) (2006) 282–286.
[25] J. Liang, Y. Huang, L. Zhang, Y. Wang, Y. Ma, T. Guo, Y. Chen, Molecular-level dispersion of graphene into poly(vinyl alcohol) and effective reinforcement of their nanocomposites, Adv. Funct. Mater 19 (14) (2009) 2297–2302.
[26] J. Wang, Q. Cheng, L. Lin, L. Chen, L. Jiang, Understanding the relationship of performance with nanofiller content in the biomimetic layered nanocomposites, Nanoscale 5 (14) (2013) 6356–6362.
[27] M. Bhattacharya, Polymer Nanocomposites-A Comparison between carbon nanotubes, graphene, and clay as nanofillers, Materials 9 (4) (2016).
[28] U.G. Wegst, H. Bai, E. Saiz, A.P. Tomsia, R.O. Ritchie, Bioinspired structural materials, Nat. Mater 14 (1) (2015) 23–36.
[29] J. Wang, Q. Cheng, Z. Tang, Layered nanocomposites inspired by the structure and mechanical properties of nacre, Chem. Soc. Rev. 41 (17) (2012) 1111–1129.
[30] S. Gong, H. Ni, L. Jiang, Q. Cheng, Learning from nature: constructing high performance graphene-based nanocomposites, Mater. Today 20 (4) (2017) 210–219.
[31] P. Laaksonen, A. Walther, J.M. Malho, M. Kainlauri, O. Ikkala, M.B. Linder, Genetic engineering of biomimetic nanocomposites: diblock proteins, graphene, and nanofibrillated cellulose, Angew. Chem. Int. Ed. 50 (2011) 8688–8691.
[32] Q. Cheng, M. Li, L. Jiang, Z. Tang, Bioinspired layered composites based on flattened double-walled carbon nanotubes, Adv. Mater 24 (14) (2012) 1838–1843.
[33] J. Wang, Q. Cheng, L. Lin, L. Jiang, Synergistic toughening of bioinspired poly(vinyl alcohol)–clay–nanofibrillar cellulose artificial nacre, ACS Nano 8 (3) (2014) 2739–2745.
[34] R.O. Mäkiniemi, P. Das, D. Hönders, K. Grygiel, D. Cordella, C. Detrembleur, J. Yuan, A. Walther, Conducting, self-assembled, nacre-mimetic polymer/clay nanocomposites, ACS Appl. Mater. Interfaces 7 (2015) 15681–15685.
[35] H.B. Yao, H.Y. Fang, Z.H. Tan, L.H. Wu, S.H. Yu, Biologically inspired, strong, transparent, and functional layered organic-inorganic hybrid films, Angew. Chem. Int. Ed. 49 (12) (2010) 2140–2145.
[36] L.J. Bonderer, A.R. Studart, L.J. Gauckler, Bioinspired design and assembly of platelet reinforced polymer films, Science 319 (5866) (2008) 1069–1073.
[37] X.Q. Li, H.C. Zeng, Calcium carbonate nanotablets: bridging artificial to natural nacre, Adv. Mater 24 (47) (2012) 6277–6282.
[38] P.M. Ajayan, J.M. Tour, Materials science—nanotube composites, Nature 447 (7148) (2007) 1066–1068.
[39] P. Podsiadlo, A.K. Kaushik, E.M. Arruda, A.M. Waas, B.S. Shim, J. Xu, H. Nandivada, B.G. Pumplin, J. Lahann, A. Ramamoorthy, Ultrastrong and stiff layered polymer nanocomposites, Science 318 (5847) (2007) 80–83.
[40] Y.Q. Li, T. Yu, T.Y. Yang, L.X. Zheng, K. Liao, Bio-inspired nacre-like composite films based on graphene with superior mechanical, electrical, and biocompatible properties, Adv. Mater 24 (25) (2012) 3426–3431.
[41] S. Park, K.S. Lee, G. Bozoklu, W. Cai, S.T. Nguyen, R.S. Ruoff, Graphene oxide papers modified by divalent ions-enhancing mechanical properties *via* chemical cross-linking, ACS Nano 2 (3) (2008) 572–578.
[42] Y. Gao, L.Q. Liu, S.Z. Zu, K. Peng, D. Zhou, B.H. Han, Z. Zhang, The effect of interlayer adhesion on the mechanical behaviors of macroscopic graphene oxide papers, ACS Nano 5 (3) (2011) 2134–2141.
[43] H.Z. Geng, R. Rosen, B. Zheng, H. Shimoda, L. Fleming, J. Liu, O. Zhou, Fabrication and properties of composites of poly(ethylene oxide) and functionalized carbon nanotubes, Adv. Mater 14 (19) (2002) 1387–1390.
[44] K. Kalaitzidou, H. Fukushima, L.T. Drzal, A new compounding method for exfoliated graphite–polypropylene nanocomposites with enhanced flexural properties and lower percolation threshold, Compos. Sci. Technol. 67 (10) (2007) 2045–2051.
[45] Z. Xu, C. Gao, In situ polymerization approach to graphene-reinforced nylon-6 composites, Macromolecules 43 (16) (2010) 6716–6723.
[46] M.M. And, K.I. Winey, Polymer nanocomposites containing carbon nanotubes, Macromolecules 39 (16) (2006) 543–545.
[47] J. Jang, J. Bae, S.H. Yoon, A study on the effect of surface treatment of carbon nanotubes for liquid crystalline epoxide–carbon nanotube composites, J. Mater. Chem. 13 (4) (2003) 676–681.
[48] R. Verdejo, M.M. Bernal, L.J. Romasanta, M.A. Lopezmanchado, Graphene filled polymer nanocomposites, J. Mater. Chem. 21 (21) (2010) 3301–3310.
[49] W. Gacitua, A. Ballerini, J. Zhang, Polymer nanocomposites: synthetic and natural fillers a review, Maderas-Cienc. Tecnol. 7 (3) (2005) 159–178.
[50] B.A. Bhanvase, S.H. Sonawane, Ultrasound assisted in situ emulsion polymerization for polymer nanocomposite: a review, Chem. Eng. Process 85 (2014) 86–107.
[51] E.C. Lee, D.F. Mielewski, R.J. Baird, Exfoliation and dispersion enhancement in polypropylene nanocomposites by in-situ melt phase ultrasonication, Polym. Eng. Sci. 44 (44) (2004) 1773–1782.
[52] G. Carotenuto, A. Yieshein Her, E. Matijević, Preparation and characterization of nanocomposite thin films for optical devices, Ind. Eng. Chem. Res. 35 (9) (1996) 575–582.
[53] M. Trujillo, M.L.A. And, A.J. Müller, E. Laredo, S. Bredeau, A.D. Bonduel, P. Dubois, Thermal and morphological characterization of nanocomposites prepared by in-situ polymerization of high-density polyethylene on carbon nanotubes, Macromolecules 40 (17) (2007) 6268–6276.
[54] J. Kwon, H. Kim, Comparison of the properties of waterborne polyurethane/multiwalled carbon nanotube and acid-treated multiwalled carbon nanotube composites prepared by in situ polymerization, J. Polym. Sci. Part A Polym. Chem. 43 (17) (2005) 3973–3985.
[55] X. Ma, B. Zhou, Y. Deng, Y. Sheng, C. Wang, Y. Pan, Z. Wang, Study on CaCO3/PMMA nanocomposite microspheres by soapless emulsion polymerization, Colloid Surf. A 312 (2–3) (2008) 190–194.
[56] S. Abedi, M. Abdouss, A review of clay-supported Ziegler–Natta catalysts for production of polyolefin/clay nanocomposites through in situ polymerization, Appl. Catal. A-Gen 475 (5) (2014) 386–409.
[57] H. Xia, W. Qi, K. Li, G.H. Hu, Preparation of polypropylene/carbon nanotube composite powder with a solid-state mechanochemical pulverization process, J. Appl. Polym. Sci. 93 (1) (2004) 378–386.
[58] Z. Wang, Z. Liang, B. Wang, C. Zhang, L. Kramer, Processing and property investigation of single-walled carbon nanotube (SWNT) buckypaper/epoxy resin matrix nanocomposites, Compos. Part A Appl. S 35 (10) (2004) 1225–1232.
[59] E.J. García, A.J. Hart, B.L. Wardle, A.H. Slocum, Fabrication and nanocompression testing of aligned carbon-nanotube-polymer nanocomposites, Adv. Mater 19 (19) (2010) 2151–2156.
[60] B.L. Wardle, D.S. Saito, E.J. García, A.J. Hart, R.G.D. Villoria, E.A. Verploegen, Fabrication and characterization of ultrahigh-volume- fraction aligned carbon nanotube–polymer composites, Adv. Mater 20 (14) (2008) 2707–2714.

[61] L. Ci, J. Suhr, V. Pushparaj, X. Zhang, P.M. Ajayan, Continuous carbon nanotube reinforced composites, Nano Lett. 8 (9) (2008) 2762–2766.
[62] Q. Cheng, J. Wang, K. Jiang, Q. Li, S. Fan, Fabrication and properties of aligned multiwalled carbon nanotube-reinforced epoxy composites, J. Mater. Res. 23 (11) (2008) 2975–2983.
[63] Q. Cheng, J. Wang, J. Wen, C. Liu, K. Jiang, Q. Li, S. Fan, Carbon nanotube/epoxy composites fabricated by resin transfer molding, Carbon 48 (1) (2010) 260–266.
[64] K. Koziol, J. Vilatela, A. Moisala, M. Motta, P. Cunniff, M. Sennett, A. Windle, High-performance carbon nanotube fiber, Science 318 (5858) (2007) 1892–1895.
[65] X. Zhong, Y. Li, Y. Liu, X. Qiao, Y. Feng, J. Liang, J. Jin, L. Zhu, F. Hou, J. Li, Continuous multilayered carbon nanotube yarns, Adv. Mater 22 (6) (2010) 692–696.
[66] Q. Cheng, J. Bao, J.G. Park, Z. Liang, C. Zhang, B. Wang, High mechanical performance composite conductor: multi-walled carbon nanotube sheet/bismaleimide nanocomposites, Adv. Funct. Mater 19 (20) (2009) 3219–3225.
[67] Q. Cheng, B. Wang, C. Zhang, Z. Liang, Functionalized carbon-nanotube sheet/bismaleimide nanocomposites: mechanical and electrical performance beyond carbon-fiber composites, Small 6 (6) (2010) 763–767.
[68] Q. Cheng, L. Jiang, Z. Tang, Bioinspired layered materials with superior mechanical performance, Acc. Chem. Res. 47 (4) (2014) 1256–1266.
[69] J.J. Richardson, M. Björnmalm, F. Caruso, Multilayer assembly: technology-driven layer-by-layer assembly of nanofilms, Science 6233 (348) (2015) 2491.
[70] J. Wang, L. Lin, Q. Cheng, L. Jiang, A strong bio-inspired layered PNIPAM-clay nanocomposite hydrogel, Angew. Chem. Int. Chem. 51 (19) (2012) 4676–4680.
[71] E. Munch, M.E. Launey, D.H. Alsem, E. Saiz, A.P. Tomsia, R.O. Ritchie, Tough, bio-inspired hybrid materials, Science 322 (5907) (2008) 1516–1520.
[72] C. Li, G. Shi, Functional gels based on chemically modified graphenes, Adv. Mater 26 (24) (2014) 3992–4012.
[73] B. Long, C. Wang, W. Lin, Y. Huang, J. Sun, Polyacrylamide-clay nacre-like nanocomposites prepared by electrophoretic deposition, Compos. Sci. Technol. 67 (13) (2007) 2770–2774.
[74] S. Wan, J. Peng, L. Jiang, Q. Cheng, Bioinspired graphene-based nanocomposites and their application in flexible energy devices, Adv. Mater 28 (30) (2016), 6265–6265.
[75] G. Decher, Toward layered polymeric multicomposites, Science 227 (1997) 1232–1237.
[76] G. Decher, J.D. Hong, Buildup of ultrathin multilayer films by a self-assembly process, 1 consecutive adsorption of anionic and cationic bipolar amphiphiles on charged surfaces, Makromol. Chem. Macromol. Symp. 46 (1) (1991) 321–327.
[77] B. Ding, C. Li, S. Fujita, S. Shiratori, Layer-by-layer self-assembled tubular films containing polyoxometalate on electrospun nanofibers, Colloid Surf. A 284–285 (2006) 257–262.
[78] R.R. Carballo, V.C. Orto, J.A. Hurst, A. Spiaggi, C. Bonazzola, I.N. Rezzano, Covalently attached metalloporphyrins in LBL self-assembled redox polyelectrolyte thin films, Electrochim. Acta 53 (16) (2008) 5215–5219.
[79] G. Zeng, J. Gao, S. Chen, H. Chen, Z. Wang, X. Zhang, Combining hydrogen-bonding complexation in solution and hydrogen-bonding-directed layer-by-layer assembly for the controlled loading of a small organic molecule into multilayer films, Langmuir 23 (23) (2007) 11631–11636.
[80] O. Crespobiel, B. Dordi, D.N. Reinhoudt, J. Huskens, Supramolecular layer-by-layer assembly: alternating adsorptions of guest- and host-functionalized molecules and particles using multivalent supramolecular interactions, J. Am. Chem. Soc. 127 (20) (2005) 7594–7600.
[81] K. Hamada, T. Serizawa, T. Kitayama, N. Fujimoto, K. Hatada, M. Akashi, Stepwise stereocomplex assembly of isotactic poly(methyl methacrylate) and syndiotactic poly(alkyl methacrylate)s on surfaces, Langmuir 17 (18) (2001) 5513–5519.
[82] H. Chen, G. Zhang, Z. Wei, K.M. Cooke, J. Luo, Layer-by-layer assembly of sol–gel oxide 'Glued' montmorillonite–zirconia multilayers, J. Mater. Chem. 20 (23) (2010) 4925–4936.
[83] E.R. Kleinfeld, G.S. Ferguson, Stepwise formation of multilayered nanostructural films from macromolecular precursors, Science 265 (5170) (1994) 370.
[84] Z. Tang, N.A. Kotov, S. Magonov, B. Ozturk, Nanostructured artificial nacre, Nat. Mater 2 (6) (2003) 413–418.
[85] L.J. Bonderer, A.R. Studart, L.J. Gauckler, Bioinspired design and assembly of platelet reinforced polymer films, Science 319 (5866) (2008) 1069–1073.
[86] R. Xiong, K. Hu, A.M. Grant, R. Ma, W. Xu, C. Lu, X. Zhang, V.V. Tsukruk, Ultrarobust transparent cellulose nanocrystal-graphene membranes with high electrical conductivity, Adv. Mater 28 (7) (2016) 1501–1509.
[87] P. Das, S. Schipmann, J.M. Malho, B. Zhu, U. Klemradt, A. Walther, Facile access to large-scale, self-assembled, nacre-inspired, high-performance materials with tunable nanoscale periodicities, ACS Appl. Mater. Inter 5 (9) (2013) 3738–3747.
[88] W. Cui, M. Li, J. Liu, B. Wang, C. Zhang, L. Jiang, Q. Cheng, A strong integrated strength and toughness artificial nacre based on dopamine cross-linked graphene oxide, ACS Nano 8 (9) (2014) 9511–9517.
[89] M. Morits, T. Verho, J. Sorvari, V. Liljeström, M.A. Kostiainen, A.H. Gröschel, O. Ikkala, Toughness and fracture properties in nacre-mimetic clay/polymer nanocomposites, Adv. Funct.l Mater 27 (10) (2017).
[90] J.M. Malho, P. Laaksonen, Walther, A. Walther, O. Ikkala, M.B. Linder, Facile method for stiff, tough, and strong nanocomposites by direct exfoliation of multilayered graphene into native nanocellulose matrix, Biomacromolecules 13 (2012) 1093–1099.
[91] A. Walther, I. Bjurhager, J.M. Malho, J. Pere, J. Ruokolainen, L.A. Berglund, O. Ikkala, Large-area, lightweight and thick biomimetic composites with superior material properties via fast, economic, and green pathways, Nano Lett. 10 (8) (2010) 2742–2748.
[92] A. Walther, I. Bjurhager, J.M. Malho, J. Ruokolainen, L. Berglund, O. Ikkala, Supramolecular control of stiffness and strength in lightweight high-performance nacre-mimetic paper with fire-shielding properties, Angew. Chem. Int. Ed. 49 (36) (2010) 6448–6453.
[93] S. Wan, H. Hu, J. Peng, Y. Li, Y. Fan, L. Jiang, Q. Cheng, Nacre-inspired integrated strong and tough reduced graphene oxide-poly(acrylic acid) nanocomposites, Nanoscale 8 (10) (2016) 5649–5656.
[94] S. Wan, Y. Li, J. Peng, H. Hu, Q. Cheng, L. Jiang, Synergistic toughening of graphene oxide-molybdenum disulfide-thermoplastic polyurethane ternary artificial nacre, ACS Nano 9 (1) (2015) 708–714.
[95] S. Gong, C. Wei, Z. Qi, A. Cao, J. Lei, Q. Cheng, Integrated ternary bioinspired nanocomposites *via* synergistic toughening of reduced graphene oxide and double-walled carbon nanotubes, ACS Nano 12 (9) (2016) 11568–11573.
[96] S. Gong, M. Wu, L. Jiang, Q. Cheng, Integrated ternary artificial nacre *via* synergistic toughening of reduced graphene oxide/double-walled carbon nanotubes/poly(vinyl alcohol), Mater. Res. Express 7 (3) (2016) 075002.
[97] A. Macchetta, I.G. Turner, C.R. Bowen, Fabrication of HA/TCP scaffolds with a graded and porous structure using a camphene-based freeze-casting method, Acta Biomater. 5 (4) (2009) 1319–1327.
[98] S. Deville, E. Saiz, R.K. Nalla, A.P. Tomsia, Freezing as a path to build complex composites, Science 311 (5760) (2006) 515–518.
[99] Y. Zhang, L. Hu, J. Han, Z. Jiang, Freeze casting of aqueous alumina slurries with glycerol for porous ceramics, Ceram. Int. 36 (2) (2010) 617–621.
[100] Q. Cheng, L. Jiang, Mimicking nacre by ice templating, Angew. Chem. Int. Ed. 56 (2017) 934–935.
[101] Q. Cheng, L. Jiang, Science behind nacre: matrix-directed mineralization at ambient condition, Sci. China. Mater 59 (11) (2016) 889–891.
[102] H. Bai, Y. Chen, B. Delattre, A.P. Tomsia, R.O. Ritchie, Bioinspired large-scale aligned porous materials assembled with dual temperature gradients, Sci. Adv. 1 (11) (2015) e1500849.
[103] L. Mao, H. Gao, H. Yao, L. Liu, H. Cölfen, G. Liu, S. Chen, S. Li, Y. Yan, Y. Liu, Synthetic nacre by predesigned matrix-directed mineralization, Science 354 (6308) (2016).
[104] H. Bai, C. Li, X. Wang, G. Shi, On the gelation of graphene oxide, J. Phys. Chem. C 115 (13) (2011) 5545–5551.
[105] Z. Xiong, C. Liao, W. Han, X. Wang, Mechanically tough large-area hierarchical porous graphene films for high-performance flexible supercapacitor applications, Adv. Mater 27 (30) (2015) 4469–4475.
[106] M. Zhang, L. Huang, J. Chen, C. Li, G. Shi, Ultratough, ultrastrong, and highly conductive graphene films with arbitrary sizes, Adv. Mater 26 (45) (2014) 7588–7592.
[107] T.H. Lin, W.H. Huang, I.K. Jun, P. Jiang, Bioinspired assembly of colloidal nanoplatelets by electric field, Chem. Mater 21 (10) (2009) 2039–2044.
[108] W. Lin, C.A. Wang, H. Le, B. Long, Y. Huang, Special assembly of laminated nanocomposite that mimics nacre, Mater. Sci. Eng.C 28 (7) (2008) 1031–1037.
[109] S. Wang, Z. Liang, T. Liu, B. Wang, C. Zhang, Effective amino-functionalization of carbon nanotubes for reinforcing epoxy polymer composites, Nanotechnology 17 (6) (2006) 1551–1557.
[110] P.C. Ma, N.A. Siddiqui, G. Marom, J.K. Kim, Dispersion and functionalization of carbon nanotubes for polymer-based nanocomposites: a review, Compos. Part A 41 (10) (2010) 1345–1367.
[111] P.C. Ma, S.Y. Mo, B.Z. Tang, J.K. Kim, Dispersion, interfacial interaction and re-agglomeration of functionalized carbon nanotubes in epoxy composites, Carbon 48 (6) (2010) 1824–1834.
[112] H. Jin, A. Cao, E. Shi, J. Seitsonen, L. Zhang, R.H.A. Ras, L.A. Berglund, M. Ankerfors, A. Waltherf, O. Ikkala, Ionically interacting nanoclay and nanofibrillated cellulose lead to tough bulk nanocomposites in compression by forced self-assembly, J. Mater. Chem. B 1 (2013) 835–840.
[113] P. Das, J.M. Malho, K. Rahimi, F.H. Schacher, B. Wang, D.E. Demco, A. Walther, Nacre-mimetics with synthetic nanoclays up to ultrahigh aspect ratios, Nat. Commun. 6 (5967) (2015).
[114] D.A. Dikin, S. Stankovich, E.J. Zimney, R.D. Piner, G.H. Dommett, G. Evmenenko, S.T. Nguyen, R.S. Ruoff, Preparation and characterization of graphene oxide paper, Nature 448 (7152) (2007) 457–460.
[115] C.N. Yeh, K. Raidongia, J. Shao, Q. Yang, J. Huang, On the origin of the stability of graphene oxide membranes in water, Nat. Chem. 7 (2) (2015) 166–170.
[116] P. Das, A. Walther, Ionic supramolecular bonds preserve mechanical properties and enable synergetic performance at high humidity in water-borne, self-assembled nacre-mimetics, Nanoscale 5 (19) (2013) 9348–9356.
[117] T. Verho, M. Karesoja, P. Das, L. Martikainen, R. Lund, A. Alegría, A. Walther, O. Ikkala, Hydration and dynamic state of nanoconfined polymer layers govern toughness in nacre-mimetic nanocomposites, Adv. Mater 25 (2013) 5055–5059.
[118] K. Chen, J. Ding, S. Zhang, X. Tang, Y. Yue, L. Guo, A general bioinspired, metals-based synergic cross-linking strategy toward mechanically enhanced materials, ACS Nano 11 (3) (2017) 2835–2845.

[119] X. Zhang, Y. Feng, S. Tang, W. Feng, Preparation of a graphene oxide–phthalocyanine hybrid through strong π–π interactions, Carbon 48 (1) (2010) 211–216.
[120] Z. An, O.C. Compton, K.W. Putz, L.C. Brinson, S.T. Nguyen, Bio-inspired borate cross-linking in ultra-stiff graphene oxide thin films, Adv. Mater 23 (33) (2011) 3842–3846.
[121] Q. Cheng, M. Wu, M. Li, L. Jiang, Z. Tang, Ultratough artificial nacre based on conjugated cross-linked graphene oxide, Angew. Chem. Int. Ed. 52 (13) (2013) 3750–3755.
[122] X. Hu, Z. Xu, Z. Liu, C. Gao, Liquid crystal self-templating approach to ultrastrong and tough biomimic composites, Sci. Rep. 3 (32) (2013), 2374–2374.
[123] P. Ming, Y. Zhang, J. Bao, G. Liu, Z. Li, L. Jiang, Q. Cheng, Bioinspired highly electrically conductive graphene-epoxy layered composites, Rsc Adv. 5 (28) (2015) 22283–22288.
[124] Q. Cheng, J. Duan, Q. Zhang, L. Jiang, Learning from nature: constructing integrated graphene-based artificial nacre, ACS Nano 9 (3) (2015) 2231–2234.
[125] L. Martikainen, A. Walther, J. Seitsonen, L. Berglund, O. Ikkala, Deoxyguanosine phosphate mediated sacri ficial bonds promote synergistic mechanical properties in nacre-mimetic nanocomposites, Biomacromolecules 14 (2013) 2531–2535.
[126] P. Song, Z. Xu, Y. Wu, Q. Cheng, Q. Guo, H. Wang, Super-tough artificial nacre based on graphene oxide *via* synergistic interface interactions of π-π stacking and hydrogen bonding, Carbon 111 (2017) 807–812.
[127] Q. Zhang, S. Wan, L. Jiang, Q. Cheng, Bioinspired robust nanocomposites of cooper ions and hydroxypropyl cellulose synergistic toughening graphene oxide, Sci. China. Technol. Sci. (2016) 1–7.
[128] A.B. Dichiara, T.J. Sherwood, J. Benton-Smith, J.C. Wilson, S.J. Weinstein, R.E. Rogers, Free-standing carbon nanotube/graphene hybrid papers as next generation adsorbents, Nanoscale 6 (12) (2014) 6322–6327.
[129] S. Wan, J. Peng, Y. Li, H. Hu, L. Jiang, Q. Cheng, Use of synergistic interactions to fabricate strong, tough, and conductive artificial nacre based on graphene oxide and chitosan, ACS Nano 9 (10) (2015) 9830–9836.
[130] S.M. Lee, E. Pippel, U. Gsele, C. Dresbach, Y. Qin, C.V. Chandran, T. Bruniger, G. Hause, M. Knez, Greatly increased toughness of infiltrated spider silk, Science 324 (5926) (2009) 488.
[131] S. Gong, L. Jiang, Q. Cheng, Robust bioinspired graphene-based nanocomposites *via* synergistic toughening of zinc ions and covalent bonding, J. Mater. Chem. A 4 (2016) 17073–17079.
[132] S. Wan, F. Xu, L. Jiang, Q. Cheng, Superior fatigue resistant bioinspired graphene-based nanocomposite *via* synergistic interfacial interactions, Adv. Funct. Mater 27 (10) (2017) 1605636.
[133] Y. Zhang, Y. Li, P. Ming, Q. Zhang, T. Liu, L. Jiang, Q. Cheng, Ultrastrong bioinspired graphene-based fibers *via* synergistic toughening, Adv. Mater 28 (14) (2016).
[134] J. Duan, S. Gong, Y. Gao, X. Xie, L. Jiang, Q. Cheng, Bioinspired ternary artificial nacre nanocomposites based on reduced graphene oxide and nanofibrillar cellulose, ACS Appl. Mater. Inter 8 (2016) 10545–10550.
[135] X. Huang, Z. Zeng, H. Zhang, Metal dichalcogenide nanosheets: preparation, properties and applications, Chem. Soc. Rev. 42 (5) (2013) 1934–1946.
[136] P. Ming, Z. Song, S. Gong, Y. Zhang, J. Duan, Q. Zhang, L. Jiang, Q. Cheng, Nacre-inspired integrated nanocomposites with fire retardant properties by graphene oxide and montmorillonite, J. Mater. Chem. A 3 (42) (2015) 21194–21200.
[137] M. Hu, B. Mi, Enabling Graphene oxide nanosheets as water separation membranes, Environ. Sci. Technol. 47 (8) (2013) 3715–3723.
[138] Y. Huang, X. Dong, Y. Shi, C. Li, L. Li, P. Chen, Nanoelectronic biosensors based on CVD grown graphene, Nanoscale 2 (8) (2010) 1485.
[139] X. Lu, H. Dou, C. Yuan, S. Yang, L. Hao, F. Zhang, L. Shen, L. Zhang, X. Zhang, Polypyrrole/carbon nanotube nanocomposite enhanced the electrochemical capacitance of flexible graphene film for supercapacitors, J. Power Sources 197 (2012) 319–324.
[140] X. Xie, L. Qu, C. Zhou, Y. Li, J. Zhu, H. Bai, G. Shi, L. Dai, An asymmetrically surface-modified graphene film electrochemical actuator, ACS Nano 4 (10) (2010) 6050–6054.
[141] Z. Yin, S. Sun, T. Salim, S. Wu, X. Huang, Q. He, Y.M. Lam, H. Zhang, Organic photovoltaic devices using highly flexible reduced graphene oxide films as transparent electrodes, ACS Nano 4 (9) (2010) 5263–5268.
[142] W. Song, M. Cao, M. Lu, S. Bi, C. Wang, J. Liu, J. Yuan, L. Fan, Flexible graphene/polymer composite films in sandwich structures for effective electromagnetic interference shielding, Carbon 66 (2014) 67–76.
[143] T. Guo, L. Heng, M. Wang, J. Wang, L. Jiang, Robust underwater oil-repellent material inspired by columnar nacre, Adv. Mater 28 (38) (2016) 8505–8510.
[144] Y. Shao, J. Wang, H. Wu, J. Liu, I.A. Aksay, Y. Lin, Graphene based electrochemical sensors and biosensors: a review, Electroanalysis 22 (10) (2010) 1027–1036.
[145] Y. Liu, X. Dong, P. Chen, Biological and chemical sensors based on graphene materials, Chem. Soc. Rev. 41 (6) (2012) 2283–2307.
[146] L. Xie, Y. Zhang, F. Gao, Q. Wu, P. Xu, S. Wang, N. Gao, Q. Wang, A highly sensitive dopamine sensor based on a polyaniline/reduced graphene oxide/nafion nanocomposite, Chin. Chem. Lett. 28 (2016) 41–48.